

Contour integral based Rayleigh-Ritz method for large-scale nonlinear eigenvalue problems

Jinyou Xiao^{a,b}, Shuangshuang Meng^a, Chuanzeng Zhang^{c,*}, Changjun Zheng^d

^a*School of Astronautics, Northwestern Polytechnical University, Xi'an 710072, China*

^b*Institute for Computational Mechanics and Its Applications, Northwestern Polytechnical University, Xi'an 710072, China*

^c*Department of Civil Engineering, University of Siegen, D-57068 Siegen, Germany*

^d*Institute of Sound and Vibration Research, Hefei University of Technology, Hefei, 230009, China*

Abstract

The robust and reliable solution of large-scale nonlinear eigenvalue problems (NEPs) in computational science and engineering is a challenging task. This paper proposes a new algorithm, denoted by CIRR(S), that utilizes the Rayleigh-Ritz procedure to compute all eigenvalues (and the corresponding eigenvectors) lying within a given contour in the complex plane. The main novelties are the following. First and foremost, the eigenspace is directly constructed by using the values of the resolvent at a series of sampling points on the contour, as such the unreliability caused by the use of high order contour moments of the resolvent in the current scheme can be effectively circumvented. Next, the projected NEP is solved by using the Sakurai-Sugiura algorithm. To enhance the reliability and accuracy, the user-defined probing matrix in the original algorithm is avoided and strategies for automatically determining the number of eigenvalues are provided. Finally, the CIRR(S) is extended to solve NEPs in the boundary element method which are hard to solve due to the densely populated matrix and high computational cost. The Chebyshev interpolation technique is used for approximating the projected matrix. The good performance of the CIRR(S) algorithm is verified by a variety of NEPs in engineering applications, with the degrees of freedom ranging from several hundreds to around one million. The algorithm is suitable for parallelization and easy to implement in conjunction with other programs and softwares.

Keywords:

nonlinear eigenvalue problems, contour integral method, eigenvalue and eigenvector, finite element method, boundary element method

1. Introduction

The natural frequency λ and natural mode v are important parameters in the design of engineering structures and systems. Mathematically, they are the eigenvalue and the corresponding eigenvector satisfying the eigen-equation

$$T(\lambda)v = 0, \quad (1)$$

where $T(z) \in \mathbb{C}^{n \times n}$ is a matrix-valued function depending on a parameter $z \in \mathcal{D} \subset \mathbb{C}$. When the matrix T in terms of z is nonlinear, (1) becomes the so-called nonlinear eigenvalue problem (NEP). Except for the quadratic eigenvalue problem that has been well-studied in the dynamic analysis of structures [1], the numerical solution of general NEPs is so far a challenging task, especially at large scales [2, 3].

This work is concerned with developing efficient numerical methods for large-scale NEPs. In particular, we consider NEPs in the *finite element method* (FEM) and the *boundary element method* (BEM) as examples.

*Corresponding author

Email addresses: xiao jy@nwpu.edu.cn (Jinyou Xiao), c.zhang@uni-siegen.de (Chuanzeng Zhang), cjzheng@hfut.edu.cn (Changjun Zheng)

These two methods are extensively applied in computational science and engineering, either independently or in coupled manners [4, 5]. Their NEPs reflect the main bottlenecks in the current development of numerical methods for NEPs. In the FEM, NEPs are often caused by the z -dependent material properties and boundary conditions; examples include the analysis of structures involving viscoelastic materials [6, 7, 8], free vibration of plates and shells with elastically attached masses [9], vibrations of fluid-solid structures [10], special treatment of artificial boundary conditions [11], etc. Typically, the FEM matrix T is sparse, symmetric, real and positive or semi-positive definite. These properties greatly benefit the numerical treatment. However, in the BEM the situation is totally different. The eigenvalue problems are in general strongly nonlinear even if the underlying physical problem is linear [12, 13, 14]. The matrix T is typically complex, dense and unstructured, making the evaluation of T itself and the operations with T (e.g., applying to vectors, solving linear systems, etc) computationally very expensive. Besides, the entries of T are usually distinct functions of z whose dependence on z cannot, at least easily, be expressed by explicit formulas. All these factors make the NEPs in the BEM very hard to be solved even with the state-of-the-art techniques [15, 16]. Similar difficulties also exist in NEPs from the coupled FEM-BEM [17, 5].

In order to meet the requirements of the aforementioned large-scale engineering applications, we aim at developing a numerical solver that simultaneously satisfies the following two requirements:

- R1*: can robustly and reliably compute all the eigenvalues (and the corresponding eigenvectors) within a given region in the complex plane.
- R2*: can solve large NEPs (e.g., degrees of freedom n up to several millions) no matter the matrix T is dense or sparse, structured or unstructured, and allows for an easy implementation and efficient parallelization.

We notice that although there exist a number of algorithms for the solution of NEPs (see e.g., [2, 18, 19, 20, 21, 16]), most of them are excluded by the above two requirements.

Essentially, existing numerical approaches for NEPs fall into three categories [2, 22]. The first and classical approach is to formulate the NEP as a system of nonlinear equations and to use variations of Newton's method. Examples include the residual inverse iteration method [23], the Jacobi-Davidson method [24, 19] and the block Newton method [20]. Typically, Newton type methods are only locally convergent and need good initial guess of the eigenvalues. The Jacobi-Davidson method can be used to determine several eigenvalues subsequently. But special strategies have to be used to avoid the repeated convergence towards the same eigenvalues [19, 20]. Recently, a deflation strategy based on the concept of minimal invariant pairs has been proposed and developed into the Jacobi-Davidson method for the robust and successive computation of several eigenpairs [16]. However, one should notice that, in all these methods, the repeated solution of the *correction equation* during the iterative process can be computational very expensive in large scales. Newton type methods applied to small BEM eigenvalue problems can be found in, e.g., [25].

The second approach is to transform the NEP into a linear eigenvalue problem which can then be solved by a solver for linear problems. This represents a standard approach in solving quadratic eigenvalue problems in the FEM [1]. The application of this approach to NEPs in the BEM can be found in [13]. In recent years, linearization by the polynomial interpolation of $T(z)$ has attracted increasing attentions in solving medium and large NEPs; see, e.g., [15, 22, 26]. But, there is still a need to construct linearizations that reflect the structure of the given matrix polynomial and to improve the stability of the linearizations [1, 27]. Moreover, in the linearization the size of the problem is many times increased, leading to considerable computational time and memory requirements in solving the linearized problem. The situation can readily become unaffordable in the BEM even when the fast BEM techniques are used, because the storage of all the $n \times n$ coefficient matrices of $T(z)$ in a polynomial basis, even in compressed forms [28], would require huge memory in large scales.

The third approach, called *contour integral method* in this paper, is based on the contour integral of the resolvent operator $T(z)^{-1}$ applied to a full-rank matrix $U \in \mathbb{C}^{n \times L}$. This approach is first developed for solving generalized eigenvalue problems [29, 30]. Later, it is extended to solving NEPs in [31] and [21], respectively, using the Smith form and Keldysh's theorem for analytic matrix-valued functions. Since [31] and [21] come up with similar algorithms, we consider the block Sakurai-Sugiura (SS) algorithm proposed in [31]. In this algorithm, the original NEP is transform into a small-sized generalized eigenvalue problem

involving block Hankel matrices, by using the monomial moments of the matrix $T(z)^{-1}U$ on a given contour. Applications of the block SS algorithm for solving NEPs in the BEM can be found in [14, 32, 33, 34]. The algorithm should be efficient in solving general NEPs under the conditions: (1) the number of columns of U , i.e., L , is sufficiently large, and (2) the contour integrals are accurately evaluated. Otherwise, the algorithm would become unreliable and inaccurate [35, 36], and loss of eigenvalues and spurious eigenvalues may frequently occur. But meeting these conditions, if possible, often implies heavy computational burdens in large-scale applications.

Although still under development, the contour integral method appears to be a very promising candidate that potentially meet the above two requirements *R1* and *R2*. It simultaneously considers all eigenvalues within a given contour; the most computationally intensive part, i.e., the solution of a series of independent linear systems, can be effectively parallelized. The main problem is how to enhance the robustness and accuracy while still keeping the computational cost to a reasonable level. Along this line, a new algorithm for solving NEPs has been recently proposed in [36] based on the Rayleigh-Ritz procedure, but using the contour integral method to generate eigenspaces. More specifically, the eigenspace is spanned by the column space of a matrix $\hat{M} \in \mathbb{C}^{n \times KL}$ collecting all the monomial moments of $T(z)^{-1}U$ up to order K on a given contour. We call this the *moment scheme* for generating eigenspaces, and denote the algorithm proposed in [36] by CIRR(M) (Contour Integral based Rayleigh-Ritz procedure using Moment scheme). Primary numerical results verify that significant improvement on the the robustness and accuracy can be achieved by using the Rayleigh-Ritz procedure.

Despite the great potential, we notice that the CIRR(M) algorithm [36] suffers from the possible failure in real applications. The cause of failure is indeed simple to be understood: the eigenspace generated by the moment scheme, i.e., \hat{M} , tends to be unreliable when high order K of moments are involved, as the matrix \hat{M} would become rank-deficient and consequently the rank condition $\text{rank}(\hat{M}) \geq \bar{n}_C$ for a proper extractoin of all the \bar{n}_C eigenpairs inside a given contour \mathcal{C} will never be satisfied; see Section 3.1 for detailed reasoning, and Sections 7.1 to 7.2 for a variety of numerical evidences. Note that, besides increasing K , the condition $\text{rank}(\hat{M}) \geq \bar{n}_C$ can also be fulfilled by increasing the value of L . But bear in mind that the main computational work of the NEP solver, i.e., the computation of $T(z)^{-1}U$, is in proportion to L , thus the use of smallest L is essential for reducing the total computational cost in large-scale solutions.

To settle the possible failure in eigenspace construction, a more reliable *sampling scheme* is proposed in this paper. In this scheme, the eigenspace is spanned by the column space of a matrix $\hat{S} \in \mathbb{C}^{n \times NL}$ collecting all the matrices $T(z_k)^{-1}U$ at a series of sampling points z_k ($k = 1, \dots, N$), instead of the moments of $T(z)^{-1}U$. Although the use of quadrature points on the contour as sampling points generally performs well, we show by using the interpolation theory that the sampling points can indeed be a general set of interpolation points in the domain of interest. The sampling scheme has several advantages over the moment scheme, for example: (1) the possible failure in eigenspace construction caused by the use of high order moments is effectively remedied and the algorithm is more concise; and more importantly, (2) the eigenspace is larger than that generated from the moment scheme thus the eigensolutions can be more accurate. Besides, the sampling scheme inherits the salient features of the contour integral method, i.e., simultaneous consideration of all eigenvalues within a given contour and good parallelizability.

We come up with a contour integral based Rayleigh-Ritz procedure using sampling scheme for constructing eigenspaces, i.e., the CIRR(S) algorithm, for solving general NEPs. The projected NEP of a small size is solved by using the block SS algorithm [31]. As mentioned before, the block SS algorithm can be robust and accurate under two conditions, which are mainly a matter of computational cost. They can be easily satisfied for the reduced NEP since it is often of a very small size (e.g., several tens or hundreds). Also due to the small size of the object problems, we propose not to use the probing matrix, like U above, in the block SS algorithm but directly computing the moments of the resolvent of the reduced matrix. As such, only very low order moments are needed, greatly enhancing the robustness of the algorithm. Moreover, a strategy for automatically determining the number of the eigenvalues is also proposed.

The CIRR(S) algorithm is able to meet the previously mentioned two requirements *R1* and *R2*. It can be used to solve general NEPs no matter the matrix $T(z)$ is sparse or dense, structured or unstructured, provided that a fast linear system solver for computing $T(z_k)^{-1}U$ and an efficient routine for computing the reduced matrix of $T(z)$ are available. It permits an efficient parallelization and can be easily implemented

in conjunction with other programs or softwares. For example, by combining the CIRR(S) with the FEM software ANSYS®), we can solve FEM NEPs with more than 1 million degrees of freedom (DOF) on a Server; see examples in Section 7.3. The implementation of the CIRR(S) in the BEM is not so straightforward as in the FEM, since an explicit expression of $T(z)$ in terms of z is in general not available for the BEM. We resolve this problem by computing the Chebyshev polynomial interpolation of $T(z)$. The price to pay is a moderate increase of time, but the operation is very suitable for parallelization. Finally, we are able to solve BEM NEPs with several tens of thousands of DOF on a PC; see Section 7.2.

Finally, it is noticed that there are several methods that are specially designed for solving NEPs in the FEM. Examples include the order-reduction-iteration method and the asymptotic method; see [6, 7, 37] and the references therein. These methods typically solve a simplified problem, for example, the eigenvalues and associated eigenvectors in the desired region for undamped problems are used for the projection. They are partially heuristic since there is no guarantee that all the interested eigenvalues are captured or that the eigensolutions of the projected system are close to those of the original system [3].

The rest of this paper is organized as follows. In Section 2, basic theories of the NEP and contour integral method are briefly reviewed for completeness. In Section 3, the moment scheme and sampling scheme for constructing eigenspaces are described. By using the Rayleigh-Ritz projection, the NEP (1) is transformed into a reduced NEP of small size. A modified block SS algorithm is proposed for robust and accurate solution of the reduced NEP in Section 4. In Section 5, the CIRR(S) is extended to solve NEPs in the acoustic BEM. The CIRR(S) algorithm is summarized in Section 6, and the performance of the method is attested by a variety of representative examples in Section 7. Section 8 presents the essential conclusions of the paper.

2. Basic theory of nonlinear eigenvalue problems

Consider a holomorphic matrix-valued function $T \in \mathbb{C}^{n \times n}$ defined in an open domain $\mathcal{D} \in \mathbb{C}$, and assume that T is regular in the sense that the determinant, $\det T(z)$, does not vanish identically. According to the Keldysh theorem [38], the singular part of $T(z)^{-1}$ can be represented in terms of the generalized eigenvectors of $T(z)$ and its Hermite transpose $T(z)^H$. This fact serves as the theoretical basis for the generation of eigenspace and thus is included here for completeness. More details can be found in, e.g., [21, 36].

A holomorphic vector-valued function $v : \mathcal{D} \rightarrow \mathbb{C}^n$ is called a *root function* of T at $\lambda \in \mathcal{D}$ if

$$T(\lambda)v(\lambda) = 0, \quad v(\lambda) \neq 0.$$

The order of zero of $T(z)v(z)$ at $z = \lambda$ is called the *multiplicity* of v at λ , denoted by ν . Since v is holomorphic, it admits an expansion of form

$$v(z) = \sum_{j=0}^{\infty} (z - \lambda)^j v_j, \quad v_0 \neq 0.$$

Any vector sequence

$$(v_0, \dots, v_{\mu-1}), \quad \mu \leq \nu$$

is called a *chain of generalized eigenvectors*, v_0 is an *eigenvector*, and $v_1, \dots, v_{\mu-1}$ are *associated vectors* for v_0 of T at λ .

Denote by η the dimension of the nullspace of $T(\lambda)$, and assume that for every $l = 1, \dots, \eta$, the tuple $(v_0^l, \dots, v_{\mu_l-1}^l)$ is a chain of generalized eigenvectors of T at λ , i.e.,

$$v^l(z) = \sum_{j=0}^{\mu_l-1} (z - \lambda)^j v_j^l, \quad 1 \leq \mu_l \leq \nu_l,$$

where the vectors v_0^1, \dots, v_0^η form a basis of the nullspace of $T(\lambda)$. Then, the system of vectors

$$(v_j^l, \quad 0 \leq j \leq \mu_l - 1, \quad 1 \leq l \leq \eta)$$

is called a *canonical system of generalized eigenvectors* (CSGEs) of T at λ . Notice that the sum of multiplicities of root functions v^1, \dots, v^η is called the *algebraic multiplicity* of λ , and η is called the *geometric multiplicity* of λ .

With the notations from the above definitions, one can obtain the following theorem regarding all eigenvalues inside a compact set $C \subset \mathcal{D}$ (see [21], Corollary 2.8).

Theorem 1. *Let $C \subset \mathcal{D}$ be a compact set containing at most finitely many eigenvalues λ_k ($k = 1, \dots, n_C$) with corresponding CSGEs of T*

$$V_C = \left(v_j^{l,k}, \quad 0 \leq j \leq \mu_{l,k} - 1, 1 \leq l \leq \eta_k, k = 1, \dots, n_C \right). \quad (2)$$

Let

$$W_C = \left(w_j^{l,k}, \quad 0 \leq j \leq \mu_{l,k} - 1, 1 \leq l \leq \eta_k, k = 1, \dots, n_C \right) \quad (3)$$

be the corresponding CSGEs of T^H . Then there exists a neighborhood $C \subset \mathcal{U} \subset \mathcal{D}$ and a holomorphic matrix-valued function $R : \Omega \rightarrow \mathbb{C}^{n \times n}$ such that for all $z \in \mathcal{U} \setminus \{\lambda_1, \dots, \lambda_{n_C}\}$, there holds

$$T(z)^{-1} = \sum_{k=1}^{n_C} \sum_{l=1}^{\eta_k} \sum_{j=1}^{\mu_{l,k}} (z - \lambda_k)^{-j} \sum_{m=0}^{\mu_{l,k}-j} v_m^{l,k} \left(w_{\mu_{l,k}-j-m}^{l,k} \right)^H + R(z). \quad (4)$$

Theorem 1 indicates that the eigenvalues are the poles of $T(z)^{-1}$. By means of the residue theorem, it is possible to extract the eigenpairs inside a given contour, denoted by \mathcal{C} , by performing contour integration on \mathcal{C} . This fact leads to the contour integral algorithms in [39, 21] for solving NEPs. In this paper, we follow a more stable and accurate way, i.e., the Rayleigh-Ritz procedure, in which Theorem 1 is used to construct eigenspaces.

The Rayleigh-Ritz procedure consists of two main steps:

- (1) Generate a proper search space \mathcal{S} . Let S be an orthogonal basis of \mathcal{S} . Usually, the number of columns of S , denoted by k_S , is much smaller than the dimension n of the original NEP (1).
- (2) Compute approximate eigenpairs (λ, v) satisfying Galerkin condition

$$v \in \mathcal{S} \quad \text{and} \quad T(\lambda)v \perp \mathcal{S},$$

which is equivalent to determine eigenpairs (λ, g) of the reduced NEP

$$T_S(\lambda)g = 0, \quad (5)$$

where $T_S(z) = S^H T(z) S \in \mathbb{C}^{k_S \times k_S}$, $g \in \mathbb{C}^{k_S}$ and the superscript H denotes the conjugate transpose. Once eigenpairs (λ, g) for the reduced NEP are obtained, the corresponding eigenpairs of the original NEP (1) are given by (λ, Sg) .

The upcoming Section 3 and Section 4 will devote to the generation of eigenspaces \mathcal{S} based on Theorem 1 and the solution of the reduced NEP (5), respectively.

3. Generation of approximate eigenspaces

Now consider a contour $\mathcal{C} \subset \mathcal{D}$ and assume that T has no eigenvalues on the contour \mathcal{C} ; see Figure 1. Denote by n_C the number of different eigenvalues inside \mathcal{C} . The corresponding CSGEs of T and T^H are denoted by V_C and W_C , respectively. According to the definitions in Section 2, when counting the algebraic multiplicity, the total number of eigenvalues, denoted by \bar{n}_C , is given by

$$\bar{n}_C = \sum_{k=1}^{n_C} \sum_{l=1}^{\eta_k} \mu_{l,k}.$$

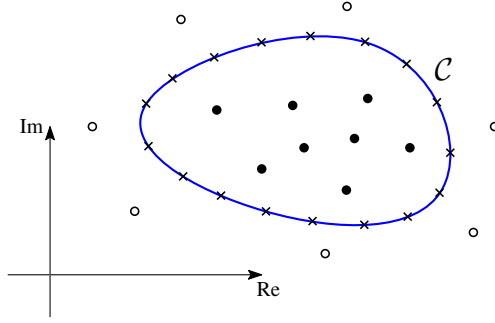


Figure 1: A diagram showing the contour \mathcal{C} (solid line), eigenvalues interested (\bullet), eigenvalues not interested (\circ) and quadrature (or sampling) points on the contour (\times).

We intend to compute all the $\bar{n}_{\mathcal{C}}$ eigenpairs inside \mathcal{C} by using the Rayleigh-Ritz procedure. To this end, we need a proper projection subspace \mathcal{S} such that $\mathcal{S} \approx \text{span}(V_{\mathcal{C}})$. Here two numerical schemes for generating \mathcal{S} according to Theorem 1 are described. The first one, the moment scheme, is first proposed in [36]. After a detailed explanation of the possible failure of the moment scheme, we propose a new sampling scheme. We will confirm that the sampling scheme can always generate more reliable eigenspace than the moment scheme.

3.1. Moment scheme

Let L be an integer larger than or equal to the maximal algebraic multiplicity of the eigenvalues of T in \mathcal{C} , i.e.,

$$L \geq \max_{k=1, \dots, n_{\mathcal{C}}} \left(\sum_{l=1}^{\eta_k} \mu_{l,k} \right),$$

and let $U \in \mathbb{C}^{n \times L}$ be a matrix with L linear independent columns. Note that usually L is a small number and is independent of n , U can be chosen as random. Then, define the moment matrices M_{α} ($\alpha = 0, 1, \dots, K'$) with respect to a set of holomorphic basis functions b_{α} (e.g., monomials in [36]) as

$$\begin{aligned} M_{\alpha} &= \frac{1}{2\pi i} \int_{\mathcal{C}} b_{\alpha}(z) T(z)^{-1} U dz \\ &= \sum_{k=1}^{n_{\mathcal{C}}} \sum_{l=1}^{\eta_k} \sum_{j=1}^{\mu_{l,k}} \frac{b_{\alpha}^{j-1}(\lambda_k)}{(j-1)!} \sum_{m=0}^{\mu_{l,k}-j} v_m^{l,k} \left(w_{\mu_{l,k}-j-m}^{l,k} \right)^H U, \end{aligned} \quad (6)$$

where the Cauchy residual theorem and relation (4) have been used to convert the contour integral in the first line into the summation in the second line, $i = \sqrt{-1}$. It is seen that each M_{α} represents a linear combination of the eigenvectors in $V_{\mathcal{C}}$; or more iconically, each M_{α} is a reflection of $V_{\mathcal{C}}$ from different angle represented by α and b_{α} . As such, it is possible to recover the space $\text{span}(V_{\mathcal{C}})$ by gathering together all the information in M_{α} . Indeed, by assuming that all algebraic operations are exact and letting

$$M = (M_0, M_1, \dots, M_{K'-1}),$$

it is easy to show that if the number K' is chosen such that

$$\text{rank}(M) = \text{rank}(V_{\mathcal{C}}), \quad (7)$$

then M contains all the information of $V_{\mathcal{C}}$, i.e.,

$$\text{span}(M) = \text{span}(V_{\mathcal{C}}).$$

This paves a way to generate eigenspace by using the moments of $T(z)^{-1}U$.

In practice, the contour integrals in (6) has to be evaluated by a numerical quadrature, resulting in approximate moments as follows

$$M_\alpha \approx \hat{M}_\alpha = \sum_{i=0}^{N-1} \omega_i b_\alpha(z_i) T(z_i)^{-1} U, \quad \alpha = 0, 1, \dots, K', \quad (8)$$

where N is the number of quadrature points, z_i and ω_i ($i = 0, \dots, N-1$) are quadrature points and weights, respectively. Then, the approximation to M is accordingly given by

$$M \approx \hat{M} = (\hat{M}_0, \hat{M}_1, \dots, \hat{M}_{K'-1}). \quad (9)$$

In some cases, one can choose K' and N such that the following rank condition is fulfilled up to some accuracy

$$\text{rank}(\hat{M}) \geq \text{rank}(V_C). \quad (10)$$

Then, one can expect $\text{span}(\hat{M})$ to be an eigenspace in the sense that

$$\text{span}(\hat{M}) \approx \text{span}(V_C).$$

The subspace $\text{span}(\hat{M})$ has been used as eigenspace in [36]. We call this the moment scheme for constructing eigenspace.

However, one should notice that the quality of eigenspace constructed by the moment scheme would deteriorate when large K' is used to “ensure” the rank condition (10). As a result, some computed eigenpairs might be of low accuracy, or more annoyingly, spurious eigenvalues and/or loss of eigenvalues might occur. The reason is that in general the columns of \hat{M} becomes more and more linearly dependent with the increase of K' and finally the condition (10) may not be fulfilled accurately.

As an illustration, we consider $b_\alpha(z) = z^\alpha$ and assume that all eigenvalues are simple so that $L = 1$ can be used. Note that in this case $n_C = \bar{n}_C$. Then the expression of M_α (6) becomes

$$M_\alpha = \sum_{k=1}^{n_C} b_\alpha(\lambda_k) v_k w_k^H U,$$

with v_k and w_k being the right and left eigenvalues of λ_k . Thus, M can be written in matrix form as

$$M = V \Lambda B$$

where $V = [v_1, \dots, v_{n_C}] \in \mathbb{C}^{n \times n_C}$, $\Lambda = \text{diag}(w)$, $w = W^H U \in \mathbb{C}^{n_C}$, $W = [w_1, \dots, w_{n_C}] \in \mathbb{C}^{n \times n_C}$ and

$$B = \begin{bmatrix} b_0(\lambda_1) & b_1(\lambda_1) & \cdots & b_{K'-1}(\lambda_1) \\ b_0(\lambda_2) & b_1(\lambda_2) & \cdots & b_{K'-1}(\lambda_2) \\ \vdots & \vdots & \ddots & \vdots \\ b_0(\lambda_{n_C}) & b_1(\lambda_{n_C}) & \cdots & b_{K'-1}(\lambda_{n_C}) \end{bmatrix}.$$

In order to effectively extract all n_C eigenvalues, the numerical rank of B , denoted by k_B , has to be equal to n_C . However, typically this condition is hard to be satisfied for relatively large n_C in case of $b_\alpha(z) = z^\alpha$, due to the fact that B is a Vandermonde matrix and becomes more and more ill-conditioned with the increase of dimensions. For example, let $n_C = 50$, then condition (10) implies that k_B has to be at less 50. Let us assume that the eigenvalues are equally distributed in interval $[-0.9, 0.9]$, which can be computed by using Matlab function `linspace(-0.9, 0.9, 50)`. Let $\sigma_1 \geq \sigma_2 \geq \dots \geq \sigma_{50}$ be the singular values of B . k_B is determined by condition that $\sigma_{k_B} \geq \text{tol} \cdot \sigma_1$ but $\sigma_{k_B+1} < \text{tol} \cdot \sigma_1$, where we set $\text{tol} = 10^{-12}$. The relation between k_B and K' for monomial basis $b_\alpha(z) = z^\alpha$ is shown by the blue solid line in Figure 2. Obviously, k_B never exceeds 35 no matter how large K' is!

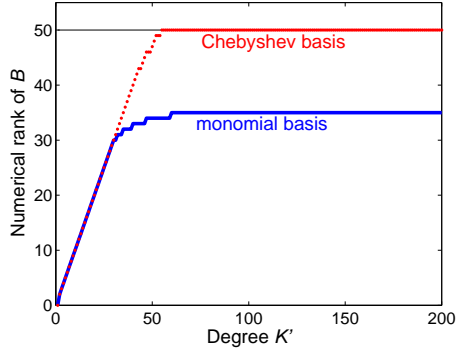


Figure 2: Numerical rank of B versus K' in monomial basis and the Chebyshev basis.

The example just given is admittedly manufactured; however, it is easy to imagine that similar situations could arise in actual applications (see Section 7). One remedy for the failure in the eigenspace generation is to choose a right set basis functions. For example, if we use Chebyshev functions of the first kind instead of the monomial functions, the condition $k_B = n_C = 50$ can be fulfilled when $K' \geq 55$; see Figure 2. However, in the next section we will propose a more general and reliable remedy in which the choices of basis functions and parameter K' are completely avoided.

3.2. Sampling scheme

The idea of the sampling scheme is inspired by the fact that each \hat{M}_α in (8) can be seen as a combination of $T(z_i)^{-1}U$, i.e.,

$$\hat{M}_\alpha = \sum_{i=0}^{N-1} c_{\alpha,i} T(z_i)^{-1}U, \quad \alpha = 0, 1, \dots, \quad (11)$$

where $c_{\alpha,i} = \omega_i b_\alpha(z_i)$ represent the combination coefficients depending on the basis functions b_α . Hence, instead of using \hat{M}_α , we generate eigenspace directly using $T(z_i)^{-1}U$. To this end, let

$$\hat{S} = [T(z_0)^{-1}U, T(z_2)^{-1}U, \dots, T(z_{N-1})^{-1}U] \in \mathbb{C}^{n \times NL}. \quad (12)$$

Then $\text{span}(\hat{S})$ is the eigenspace obtained by the *sampling scheme*. If z_i are chosen to be the quadrature points used to evaluate \hat{M}_α in (8), there holds

$$\text{span}(\hat{M}) \subseteq \text{span}(\hat{S}),$$

because \hat{M}_α is the linear combination of $T(z_i)^{-1}U$. But there is nothing in the sampling scheme (12) that constrains the sampling points z_i to be chosen according to a quadrature rule. In this sense $\text{span}(\hat{S})$ provides more general eigenspace than $\text{span}(\hat{M})$.

The sampling scheme can also be interpreted by using polynomial interpolation so that the reliance on quadrature rules is avoided. More importantly, this represents an extension of the contour integral method to more general situations. Before proceeding, we first recall some definitions from the theory of barycentric representations of polynomial interpolations [40]. The *node polynomial* for points z_0, \dots, z_{N-1} is denoted by

$$l(z) = (z - z_0)(z - z_1) \cdots (z - z_{N-1}).$$

The *barycentric weights* are denoted by

$$\omega_i = \frac{1}{l'(z_i)} = \frac{1}{\prod_{j=0, j \neq i}^{N-1} (z_i - z_j)}. \quad (13)$$

Any polynomial p of degree at most $N - 1$ can be expressed in terms of its values at points z_i using the *barycentric formula of the first kind* as

$$p(z) = l(z) \sum_{i=0}^{N-1} \frac{\omega_i p(z_i)}{z - z_i}. \quad (14)$$

Let $g[z_0, \dots, z_{N-1}]$ denote the $(N - 1)$ th divided difference of a function $g(z)$. By direct application of the Lagrange interpolation formula one has

$$g[z_0, \dots, z_{N-1}] = \sum_{i=0}^{N-1} \omega_i g(z_i). \quad (15)$$

Note that (15) gives the leading coefficient of the polynomial of degree at most $N - 1$ that takes the values $g(z_i)$ at points z_0, \dots, z_{N-1} . Clearly, if $g(z)$ is a polynomial of degree strictly less than $N - 1$, then $g[z_0, \dots, z_{N-1}]$ vanishes.

Our goal is to recover $\text{span}(V_C)$ by using the matrix-valued function $T^{-1}(z)U$. To do so, for any integer $0 \leq \alpha \leq K''$ we define the moment of $T^{-1}(z)U$ by

$$M'_\alpha = \sum_{i=0}^{N-1} \omega_i z_i^\alpha T^{-1}(z_i)U, \quad (16)$$

where the value of $K'' < N - 1$ will be clear later. Note that z_i in the definition of M'_α are interpolation points that are not eigenvalues of T . This is essentially different from the moments in (6) and (8). Since $R(z)$ in T^{-1} is holomorphic and we assume that N is large enough such that $R(z)$ can be well represented by a matrix polynomial of degree less than $N - 1 - K''$, then it follows from (15) that

$$\sum_{i=0}^{N-1} \omega_i z_i^\alpha R(z_i)U = 0, \quad \alpha = 0, \dots, K''.$$

Thus,

$$M'_\alpha = \sum_{k=1}^{n_C} \sum_{l=1}^{\eta_k} \sum_{j=1}^{\mu_{l,k}} \sum_{i=1}^N \omega_i z_i^\alpha (z_i - \lambda_k)^{-j} \sum_{m=0}^{\mu_{l,k}-j} v_m^{l,k} \left(w_{\mu_{l,k}-j-m}^{l,k} \right)^H U. \quad (17)$$

Similar to (9), the eigenspace $\text{span}(V_C)$ can be recovered by collecting all the moments M'_α together,

$$\hat{M}' = \left(\hat{M}'_0, \hat{M}'_1, \dots, \hat{M}'_{K''-1} \right). \quad (18)$$

To see the relation between \hat{M}' and $\text{span}(V_C)$, we first consider the following term in (17)

$$\phi_{\alpha,j}(\lambda) := \sum_{i=1}^N \frac{\omega_i z_i^\alpha}{(z_i - \lambda)^j}. \quad (19)$$

It follows from the polynomial interpolation equation (14) that

$$\phi_{\alpha,1}(\lambda) = \sum_{i=1}^N \frac{\omega_i z_i^\alpha}{z_i - \lambda} = -\frac{\lambda^\alpha}{l(\lambda)}. \quad (20)$$

The following relations can be obtained from (19) and (20)

$$\lambda \phi_{\alpha,1}(\lambda) = \phi_{\alpha+1,1}(\lambda), \quad \phi_{\alpha,j}(\lambda) = \frac{\phi_{\alpha,1}^{(j-1)}(\lambda)}{(j-1)!} \quad \text{and} \quad \lambda \phi_{\alpha,j}(\lambda) + \phi_{\alpha,j-1}(\lambda) = \phi_{\alpha+1,j}(\lambda). \quad (21)$$

We define two $k \times k$ matrices by

$$J_{\lambda,k} = \begin{bmatrix} \lambda & 1 & & \\ & \ddots & \ddots & \\ & & \lambda & 1 \\ & & & \lambda \end{bmatrix}, \quad \Phi_{\alpha,k} = \begin{bmatrix} \phi_{\alpha,1} & \phi_{\alpha,2} & \cdots & \phi_{\alpha,k} \\ & \ddots & \ddots & \vdots \\ & & \phi_{\alpha,1} & \phi_{\alpha,2} \\ & & & \phi_{\alpha,1} \end{bmatrix}.$$

Clearly, $J_{\lambda,k}$ is the k -dimensional Jordan block. By invoking relations in (21) one has

$$\Phi_{\alpha,k} = J_{\lambda,k} \Phi_{\alpha-1,k} = \cdots = J_{\lambda,k}^{\alpha-1} \Phi_{1,k} = J_{\lambda,k}^{\alpha} \Phi_k, \quad (22)$$

where $\Phi_k \equiv \Phi_{0,k}$. By writing (17) into matrix form and invoking relation (22), the matrix \hat{M}' in (18) becomes

$$\hat{M}' = V_{\mathcal{C}} [\Phi W_{\mathcal{C}}^H U \quad \Lambda \Phi W_{\mathcal{C}}^H U \quad \cdots \quad \Lambda^{K''} \Phi W_{\mathcal{C}}^H U], \quad (23)$$

where

$$\Lambda = \begin{bmatrix} J_1 & & \\ & \ddots & \\ & & J_{n_{\mathcal{C}}} \end{bmatrix}, \quad J_k = \begin{bmatrix} J_k^1 & & \\ & \ddots & \\ & & J_k^{\eta_k} \end{bmatrix}, \quad J_k^l = J_{\lambda_k, \mu_l, k}, \quad (24)$$

and Φ can be formulated analogously.

Equation (24) implies that if K'' is chosen such that it is of full rank, i.e.,

$$\text{rank}([\Phi W_{\mathcal{C}}^H U \quad \Lambda \Phi W_{\mathcal{C}}^H U \quad \cdots \quad \Lambda^{K''} \Phi W_{\mathcal{C}}^H U]) = \bar{n}_{\mathcal{C}}$$

then there holds

$$\text{span}(\hat{M}') = \text{span}(V_{\mathcal{C}}).$$

So eigenspace can be generated from the moments defined in (16), which is of similar form with the contour moments in (11). Since \hat{M}' is also a linear combination of $T^{-1}(z_i)U$, one can construct eigenspace directly via \hat{S} in (12). From this derivation it can be clearly seen that the sampling points z_i indeed can be a general set of interpolation points in the domain enclosed by the contour \mathcal{C} , not limiting to quadrature points on \mathcal{C} . The use of interpolation points is advantageous when the matrix T and the eigenvalues are all real. In this case if the interpolation points z_i in the real interval of the eigenvalues are used, then only real arithmetic is involved; however, the use of sampling points on a contour will require complex arithmetic, which suffers from roughly a factor of two penalty in both time and storage costs, compared with approaches that rely only on real arithmetic. This problem has been studied in [41] for standard eigenvalue problems with real symmetric matrices. In this paper, we shall not further pursue this topic, but always choose z_i to be the points of the trapezoid rule on the contour since this choice leads to good results in general situations.

For the application in the CIRRR method, an orthogonal basis of \hat{S} , denoted by S , is needed. It can be computed by the truncated SVD of \hat{S} with a tolerance δ . Usually, $\delta = 10^{-14}$ is chosen. Since the number of the columns of \hat{S} , i.e., $N \cdot L$, is typically small and independent of the size n of the problem, the computational cost of the SVD scales only linearly with n .

The eigenspace for the sampling scheme is given by $\mathcal{S} = \text{span}(S)$. Let k_S denote the numerical rank of \hat{S} obtained by the truncated SVD. In order to properly extract all the eigenvalues inside \mathcal{C} , the condition $k_S \geq \text{rank}(V_{\mathcal{C}})$ has to be satisfied. However, since $\bar{n}_{\mathcal{C}} \geq \text{rank}(V_{\mathcal{C}})$, it is more convenient to use the following condition

$$N \cdot L \geq k_S \geq \bar{n}_{\mathcal{C}}, \quad (25)$$

which means N and L have to be chosen such that k_S is larger than $\bar{n}_{\mathcal{C}}$. Our numerical experiments indicate that provided the contour is suitably chosen to enclose all the eigenvalues, there always exist moderate values of N and L to meet condition (25). Of course, L should be no less than the maximal algebraic multiplicity of the eigenvalues in \mathcal{C} . In fact, in our CIRRR method L is allowed to be equal to the maximal algebraic multiplicity of the eigenvalues.

4. Solution of the reduced NEP

Once the eigenspace is obtained, by using the standard Rayleigh-Ritz procedure the original NEP (1) is transformed into the reduced NEP (5) of size k_S , which has the same eigenvalues and multiplicities as (1). Given the eigenpairs (λ, g) of the reduced NEP, the corresponding eigenpairs of the original NEP are then given by (λ, Sg) .

The dimension of $T_S(z)$, i.e., k_S , usually ranges from several tens to several hundreds. Quite a few existing methods can be used to treating NEPs of this type. Whereas, a method that can robustly and accurately capture all eigenvalues in certain region is still lacking. The block SS algorithm proposed in [39] (see also [21]) is capable of directly computing all eigenvalues within a given contour, without needing an initial guess of their locations. But there are two important parameters left for the users to determine: one, denoted by L' , has to be larger than the maximal algebraic multiplicity of the eigenvalues inside \mathcal{C} ; another is the threshold used to truncate the singular values of the Hankel matrix H . Both the two parameters are problem dependent. Improper values of them can lead to wrong eigenvalues.

Here, we modify the block SS algorithm so that the parameter L' is avoided. Meanwhile, we come up with a strategy to determine the number of singular values of H that should be retained in the truncation, so that the need for an explicit threshold is avoided as well. The basic theories involved here can be found in [39, 21].

4.1. Moments of $T_S(z)^{-1}$

The block SS algorithm starts by computing the following moments of the matrix function $T_S(z)^{-1}$ up to order $2K - 1$

$$A_\alpha = \frac{1}{2\pi i} \int_{\mathcal{C}} \left(\frac{z - \gamma}{\rho} \right)^\alpha T_S(z)^{-1} dz, \quad \alpha = 0, 1, \dots, 2K - 1, \quad (26)$$

where K denotes the number of blocks in each row or column of the Hankel matrices; see (28). Note that: (i) here we use the same contour \mathcal{C} as the one used in generating the eigenspace in section 3; (ii) the shift and scaling parameters γ and ρ are introduced to improve the stability, and for the elliptical contour defined in (35) γ is the center of the ellipse and $\rho = \max(a, b)$; (iii) the moments are different from those used in [39] in that the random probing matrix of dimension $n \times L'$ used in [39] is not explicitly involved here, thanks to the small size of the problem. From Theorem 1 one has,

$$A_\alpha = \tilde{V} \Lambda^\alpha \tilde{W}^H, \quad (27)$$

where

$$\begin{aligned} \tilde{V} &= \left(\tilde{v}_j^{l,k}, \quad 0 \leq j \leq \mu_{l,k} - 1, 1 \leq l \leq \eta_k, 1 \leq k \leq n_C \right), \\ \tilde{W} &= \left(\tilde{w}_j^{l,k}, \quad 0 \leq j \leq \mu_{l,k} - 1, 1 \leq l \leq \eta_k, 1 \leq k \leq n_C \right) \end{aligned}$$

are the CSGEs of T_S and T_S^H defined analogously as (2) and (3). The matrix Λ has Jordan normal form similar to that in (24), but with Jordan blocks $J_k^l = J_{\lambda_k', \mu_{l,k}}$, $\lambda_k' = \frac{\lambda_k - \gamma}{\rho}$.

4.2. Transformed linear eigenvalue problem and its solution

We define two block Hankel matrices as

$$H = \begin{bmatrix} A_0 & A_1 & \cdots & A_{K-1} \\ A_1 & \ddots & \ddots & \vdots \\ \vdots & \ddots & \ddots & \vdots \\ A_{K-1} & \cdots & \cdots & A_{2K-2} \end{bmatrix}, \quad H^< = \begin{bmatrix} A_1 & A_2 & \cdots & A_K \\ A_2 & \ddots & \ddots & \vdots \\ \vdots & \ddots & \ddots & \vdots \\ A_K & \cdots & \cdots & A_{2K-1} \end{bmatrix}. \quad (28)$$

¹Notice that the parameter L' here is in fact denoted by L in [39]. It plays a similar role as the parameter L in Section 3 for generating eigenspaces.

By using (27), one has

$$H = \begin{bmatrix} \tilde{V} \\ \tilde{V}\Lambda \\ \vdots \\ \tilde{V}\Lambda^{K-1} \end{bmatrix} [\tilde{W}^H \quad \Lambda\tilde{W}^H \quad \dots \quad \Lambda^{K-1}\tilde{W}^H], \quad H^< = \begin{bmatrix} \tilde{V} \\ \tilde{V}\Lambda \\ \vdots \\ \tilde{V}\Lambda^{K-1} \end{bmatrix} \Lambda [\tilde{W}^H \quad \Lambda\tilde{W}^H \quad \dots \quad \Lambda^{K-1}\tilde{W}^H].$$

To ensure that the eigenvalue matrix Λ can be properly extracted from the matrices H and $H^<$, K has to be chosen such that

$$\text{rank} \begin{bmatrix} \tilde{V} \\ \tilde{V}\Lambda \\ \vdots \\ \tilde{V}\Lambda^{K-1} \end{bmatrix} = \text{rank} [\tilde{W}^H \quad \Lambda\tilde{W}^H \quad \dots \quad \Lambda^{K-1}\tilde{W}^H] = \bar{n}_C \quad (29)$$

holds. In most real applications, a very small K is often sufficient, e.g., $K < 10$.

To extract the eigenvalues, one first compute the truncated SVD of H ,

$$H = V\Sigma W^H \approx V_0\Sigma_0 W_0^H. \quad (30)$$

The way to obtain V_0 , Σ_0 and W_0 from V , Σ and W will be detailed later. Then we compute the matrix

$$A = V_0^H H^< W_0 \Sigma_0^{-1}, \quad (31)$$

which has the Jordan normal form Λ [21]. The eigenvalue problem for A can be easily solved by using Matlab function `eig`. Let (λ', g') be an eigenpair of A , then the corresponding eigenpair (λ, g) of the reduced NEP (5) can be obtained as

$$g = H_r W_0 \Sigma_0^{-1} g', \quad \lambda_k = \rho \lambda'_k + \gamma, \quad (32)$$

where $H_r = [A_0 \ A_1 \ \dots \ A_{K-1}]$.

4.3. Determining the number of the eigenvalues

The number of the computed eigenvalues is equal to the number of the leading singular values retained in Σ_0 . Thus a proper truncation in (30) is crucial for obtaining correct eigenpairs. In [39, 21] the authors proposed to truncate the singular values of H using a predetermined threshold tol such that the first \bar{n}_C singular values larger than tol are retained in Σ_0 ; that is, if $\sigma_1 \geq \dots \geq \sigma_{\bar{n}_C} > tol \geq \sigma_{\bar{n}_C+1} \geq \dots \geq \sigma_{K \cdot k_S}$, then $V_0 = V(1 : \bar{n}_C, :)$, $\Sigma_0 = \text{diag}(\sigma_1, \dots, \sigma_{\bar{n}_C})$, $W_0 = W(1 : \bar{n}_C, :)$. But in general the optimal threshold tol is affected by several factors, including the conditioning of the matrices in (29), the distribution of the eigenvalues and the positions of the contour, etc. As a result, it is not easy to choose it before solving the NEP.

For the solution of the reduced NEP in (5), we suggest two approaches to the determination of \bar{n}_C in automatic manner. The first approach is based on the fact that the number of eigenvalues inside \mathcal{C} is equal to the winding number

$$\bar{n}_C = \frac{1}{2\pi i} \int_{\mathcal{C}} \left[\frac{d}{dz} \log \det(T_S(z)) \right] dz = \frac{1}{2\pi i} \int_{\mathcal{C}} \text{tr} \left(T_S(z)^{-1} \frac{dT_S(z)}{dz} \right) dz, \quad (33)$$

where $\text{tr}(M)$ denotes the trace of the matrix M . Since in this paper $T_S(z)$ is expressed in form of (38), the derivative $dT_S(z)/dz$ can be computed easily. The contour integral in (33) can be computed by using quadrature rules outlined in (36).

The second approach is based on the gaps of the singular values of H in (30). We found that the largest gap between two successive singular values denoted by

$$g_{\max} = \max_{j=1, \dots, k_S-1} (\sigma_j / \sigma_{j+1}),$$

typically reaches its maximum at $j = \bar{n}_C$. This leads to the following strategy:

$$\text{if } g_{\max} \geq \text{tol}_{\text{gap}}, \quad \text{then } \bar{n}_C = \underset{j=1, \dots, k_S-1}{\text{Argmax}} (\sigma_j / \sigma_{j+1}), \quad (34)$$

where the user-defined constant tol_{gap} is introduced only to check whether a g_{\max} is reasonable; for example, we always set $\text{tol}_{\text{gap}} = 10^3$.

In practice, the two approaches can be combined to form more reliable strategies for determining \bar{n}_C . When the moments A_α in (26) are evaluated sufficiently accurate (i.e., N_S in (36) is large enough), (33) and (34) should have the same result. Otherwise, if the two approaches result in different numbers of the eigenvalues, one may need to check whether the contour is properly selected; or one can compute the eigenpairs corresponding to both the two numbers and determine which is more reasonable by checking the residual $\|T_S(\lambda)v\|_2/\|v\|_2$ for each eigenpair (λ, v) .

4.4. Algorithm for solving the reduced NEP

The procedures of the modified block SS method is summarized in Algorithm 1. In this paper, the contour is chosen from the ellipses given by the following parameterization

$$\varphi(\alpha) = \gamma + [a \cos(\alpha) + ib \sin(\alpha)], \quad \alpha \in [0, 2\pi), \quad (35)$$

where, $\gamma \in \mathbb{C}$ is the center, a and b are the lengths of the major axis and minor axis, respectively. The moments of $T_S(z)^{-1}$ in (26) are evaluated by using N_S -point trapezoid rule, leading to the following approximation

$$A_\alpha \approx \frac{1}{iN_S} \sum_{j=0}^{N_S-1} \left[\frac{\varphi(\theta_j) - \gamma}{\rho} \right]^\alpha \varphi'(\theta_j) T(\varphi(\theta_j))^{-1}, \quad \alpha = 0, 1, \dots, 2K-1, \quad (36)$$

where $\theta_j = 2\pi(j + 1/2)/N_S$, $j = 0, \dots, N_S$ are the quadrature points.

Algorithm 1: A modified block SS algorithm for solving reduced NEP (5).

- Step 1:** Choose the number of quadrature points N_S on the contour \mathcal{C} , and K that determines the number of blocks in Hankel matrices.
 - Step 2:** Compute A_α , $\alpha = 0, \dots, 2K-1$ from (26), and matrices H and $H^<$ (28).
 - Step 3:** Compute the SVD of H and determine \bar{n}_C by using the strategy in Section 4.3.
 - Step 4:** Compute the matrix A from (31), solve the corresponding standard eigenvalue problem and obtain the \bar{n}_C eigenpairs (λ, g) of the reduced NEP from (32).
-

We remark that the block SS method is also based on the theory in Section 2. In particular, following the block SS method it is possible to solve the original NEP (1) using the moments \hat{M}_α computed in (8). However, as we have pointed out in the introduction, this approach can be unstable and inaccurate when L is not very large. Bear in mind that a large L implies a high computational burden in large scales. But the situation is quite different in small scales. Since the computational cost is negligible, one can afford to choose L to be the dimension of the matrix T_S , and at the same time to use high order quadratures for the contour integration. As a result, the block SS method becomes very stable and accurate and thus an efficient approach for NEPs of small and moderate sizes.

5. An extension to NEPs in the BEM

The CIRR algorithms can be readily applied when the matrix $T(z)$ is explicitly expressed as

$$T(z) = \sum_{j=1}^J T_j f_j(z), \quad (37)$$

with T_j and $f_j(z)$ being given matrices and functions, because in this case the expression of the reduced matrix $T_S(z)$ can be easily obtained as

$$T_S(z) = \sum_{j=1}^J (S^H T_j S) f_j(z). \quad (38)$$

By assuming that the number of the terms J is much less than n (for example, less than 100), the coefficient matrices $S^H T_j S$ can then be computed with affordable computational cost. Note that the evaluation of $S^H T_j S$ is very suitable for parallelization.

However, there is a more general case where the matrix T comes not inherently in the form of (37). A typical example is the NEP in the BEM, in which the entries $T_{ij}(z)$ of $T(z)$ are different functions of z , and the explicit expressions of $T_{ij}(z)$ are difficult to obtain when singular integration is involved. Consequently, the CIR algorithms can not be directly applied. In this section, the NEP of the BEM in acoustics is taken as a model problem. After a concise review of the basic formulation of the NEP, the Chebyshev interpolation of T is used to convert it into a suitable form (37).

5.1. NEPs of BEM in acoustics

The steady-state acoustic wave pressure p at any location $\mathbf{x} \in R^3$ in a bounded domain D , enclosed by a boundary surface ∂D , is governed by the second-order Helmholtz partial differential equation

$$\nabla^2 p + z^2 p = 0, \quad (39)$$

where, z is used to denote the wavenumber, $z = \omega/c = 2\pi f/c$, and c is the speed of sound. In order to uniquely define the pressure field in the domain D , proper boundary conditions, e.g., the Dirichlet or Neumann boundary conditions, have to be specified on the closed boundary surface ∂D .

The BEM is an important numerical method for solving the Helmholtz equation. Instead of treating (39) directly, the BEM solves the following Helmholtz boundary integral equation (BIE)

$$C(\mathbf{x})p(\mathbf{x}) + \int_{\partial D} \frac{\partial F(\mathbf{x}, \mathbf{y})}{\partial n_{\mathbf{y}}} p(\mathbf{y}) d\mathbf{y} = \int_{\partial D} F(\mathbf{x}, \mathbf{y}) \frac{\partial p(\mathbf{y})}{\partial n_{\mathbf{y}}} d\mathbf{y}, \quad (40)$$

which can be obtained by using the Green's second identity to the Helmholtz PDE. In (40), $C(\mathbf{x})$ is the free term coefficient at \mathbf{x} , $n_{\mathbf{y}}$ denotes the outward normal at \mathbf{y} , $F(\mathbf{x}, \mathbf{y}) = \exp(iz|\mathbf{x} - \mathbf{y}|)/|\mathbf{x} - \mathbf{y}|$ is the fundamental solution of the Helmholtz equation in three dimensions.

In this paper, the boundary surface ∂D is discretized into curved triangular quadratic elements. The 6-node conforming quadratic element is used in the geometry approximation, and the 6-node non-conforming quadratic element is used for the approximation of the unknown functions; the nodes are the projections of the Gauss quadrature points on the reference element. The Nyström method is used to discretize the Helmholtz BIE (40), leading to the following standard discretized system in the BEM

$$H(z)u(z) = G(z)q(z),$$

where H and G are complex square matrices obtained by the Nyström discretization of the left and right side of BIE (40), respectively, u and q are vector collections of the nodal pressure p and its normal derivative $\partial p/\partial n$ which is related to the normal velocity of the acoustic media. For more details about the numerical implementation, the readers are referred to Section 2.2 of [28].

By considering the boundary conditions and gathering together the unknown quantities into a vector v , one obtains a linear system of form $T(z)v(z) = b(z)$, where b accounts for the contribution of the boundary conditions and should be set to zero in the NEP. Therefore, the BEM NEP comes into the general form (1), i.e.,

$$T(z)v = 0.$$

In accordance with (1), the dimensions of all the matrices and vectors mentioned here are denoted by n .

As the Nyström discretization based on non-conforming elements is used, the entries of H and G associated with well-separated nodes \mathbf{x}_i and \mathbf{y}_j are just the values of double- and single-layer integral kernels, that is,

$$H_{ij}(z) = \frac{\partial}{\partial n_{\mathbf{y}_j}} \frac{\exp(izr_{ij})}{r_{ij}}, \quad G_{ij}(z) = \frac{\exp(izr_{ij})}{r_{ij}}, \quad (41)$$

where $r_{ij} = |\mathbf{x}_i - \mathbf{y}_j|$. When nodes \mathbf{x}_i and \mathbf{y}_j are not well-separated, i.e., the element integral corresponds to \mathbf{x}_i and the boundary element of \mathbf{y}_j is singular or nearly singular, the expressions of $H_{ij}(z)$ and $G_{ij}(z)$ in terms of z could be much more complicated. As a result, the entries of $T(z)$ are generally distinct functions of z , and for some of them the expressions are even hard to acquire. This is an intrinsic feature of the BEM. The situations in collocation and Galerkin discretizations are even more troublesome.

In order to enable large-scale and wide frequency band solutions, the BEM in this paper is accelerated by using the fast directional multipole method, see [28].

5.2. Chebyshev interpolation of BEM matrix

Here by using Chebyshev polynomial interpolation, the matrix T is transformed into the form (37) so that the reduced matrix $T_S(z)$ can be computed with moderate computational cost.

To simplify the presentation, the eigenvalue region of interest is assumed to be the interval $[-1, 1]$. Let

$$T(z) \approx P(z) = P_0\tau_0(z) + \cdots + P_d\tau_d(z) \quad (42)$$

be a polynomial interpolation of the matrix $T(z)$ of degree d that satisfies

$$T(x_j) = P(x_j), \quad j = 0, \dots, d,$$

where τ_j are Chebyshev polynomials of order j , $x_j \in [-1, 1]$ are the Chebyshev points of the first kind, i.e.,

$$x_j = \cos(\theta_j), \quad \theta_j = \frac{j + \frac{1}{2}}{d + 1}\pi,$$

and P_j are coefficient matrices that can be computed as

$$P_j = \frac{2}{d + 1} \sum_{k=0}^d T(x_k) \cos(j\theta_k). \quad (43)$$

By combining (42), (43) and (5), one obtains

$$T_S(z) \approx P_S(z) := S^H P(z) S = \hat{P}_0\tau_0(z) + \cdots + \hat{P}_d\tau_d(z), \quad (44)$$

where the coefficient matrices $\hat{P}_j \in \mathbb{C}^{k_S \times k_S}$ are given by,

$$\hat{P}_j = \frac{2}{d + 1} \sum_{k=0}^d [S^H T(x_k) S] \cos(j\theta_k). \quad (45)$$

Thus, the coefficient matrices \hat{P}_j of the Chebyshev interpolation $P_S(z)$ can be computed by matrix-vector multiplications with the original system matrix T at Chebyshev points x_k . These operations can be efficiently parallelized.

As T is a holomorphic function on a neighborhood of the real interval $[-1, 1]$, the error of the Chebyshev interpolant in (42) decays exponentially with the degree d [15]. Thus, a moderate d is often sufficient to ensure good accuracy.

6. Summary of the proposed CIRR(S) algorithm

The CIRR(S) method proposed in this paper is summarized in Algorithm 2. The number L has to be at least not less than the algebraic multiplicity of the interested eigenvalues. In some cases (e.g., structural modal analysis) this can be estimated from the symmetry of the problems. Otherwise, one can use a large L , but this would essentially increase the computational cost for large-scale problems. As a rule-of-thumb, the number of samplings N should be chosen such that the ratio of the first to the last singular values of \hat{S} is large enough, e.g., larger than 10^{14} . This is often the case when $N \cdot L$ is more than 3 or 4 times the number of the eigenvalues \bar{n}_C . The error tolerance δ in Step 3 can always be set as $\delta = 10^{-16}$.

The CIRR(S) method can be easily implemented in conjunction with other softwares. In fact, only steps 2 and 4 involve the operations with the matrix T and can be carried out by the host softwares. Other steps can be seen as preprocessing and postprocessing parts for the host softwares. In this paper, the CIRR(S) is implemented into the FEM software ANSYS® and our fast BEM program; see the next section for numerical results.

Finally, we notice that the Rayleigh-Ritz procedure using the moment scheme, i.e., the CIRR(M) algorithm, can be implemented analogously as Algorithm 2. In this case, the parameter K has to be initialized in Step 1, and the matrix \hat{S} in Step 3 has to be replaced by \hat{M} .

Algorithm 2: The CIRR(S) algorithm for large-scale NEP (1).

- Step 1:** Choose a contour \mathcal{C} and the parameters N and L according to (25), choose a random matrix $U \in \mathbb{C}^{n \times L}$, and determine sampling points $z_i, i = 1, \dots, N$ on \mathcal{C} .
 - Step 2:** Compute $T(z_i)^{-1}U, i = 1, \dots, N$.
 - Step 3:** Formulate \hat{S} by (12). Compute the truncated SVD $\hat{S} \approx S\Sigma_0W_0^H$ such that the first k_S singular values larger than $\delta \cdot \sigma_1$ are retained. Then form the eigenspace $\mathcal{S} = \text{span}(S)$.
 - Step 4:** Compute $T_S(z) = S^HT(z)S$, and solve the reduced NEP (5) by Algorithm 1 to obtain \bar{n}_C eigenpairs $(\lambda_j, g_j), j = 1, \dots, \bar{n}_C$.
 - Step 5:** Compute the eigenpairs (λ_j, v_j) of the original NEP (1) via $(\lambda_j, Sg_j), j = 1, \dots, \bar{n}_C$.
-

7. Numerical examples

A number of examples for benchmark NEPs and those arising in real finite element and boundary element analysis are provided to demonstrate the superior performance of the CIRR(S) algorithm.

7.1. Four benchmark examples

The examples are selected from the NLEVP [42]. We solve the NEPs via CIRR(S) and CIRR(M), respectively, and compare the accuracy of the computed eigenpairs obtained from the two algorithms. The accuracy of an eigenpair (λ, v) is measured by the relative error $\|T(\lambda)v\|_2/\|v\|_2$. The first three examples belong to the quadratic eigenvalue problem which is also nonlinear. The coding and computation are conducted using Matlab R2009a. The linear systems in computing $Y_i := T(z_i)^{-1}U$ is solved by using Matlab backslash operator ‘\’ in sparse mode.

- (1) *Wiresaw*. This is a quadratic eigenvalue problem of the standard form $T(\lambda)v = (\lambda^2M + \lambda C + K)v = 0$, arising in the vibration analysis of a wiresaw. The $n \times n$ matrices are defined by

$$M = \frac{1}{2}I_n, \quad C = [c_{jk}], \quad K = \text{diag} \left(\frac{j^2\pi^2(1-\nu^2)}{2}, j = 1, \dots, n \right),$$

and $c_{jk} = 4jk\nu/(j^2 - k^2)$ if $(j + k)$ is odd, otherwise, $c_{jk} = 0$. We use $n = 500$ and $\nu = 0.01$, the corresponding matrices can be generated by using `nlevp('wiresaw1', 500, 0.01)`.

- (2) *Acoustic-1D*. This quadratic eigenvalue problem arises from the finite element discretization of the time harmonic wave equation (39) in a one-dimensional interval $[0, 1]$, where the boundary conditions are Dirichlet ($p = 0$) at one end and impedance ($q + \frac{2\pi fi}{\zeta}p = 0$) at another end. The $n \times n$ matrices are defined by

$$M = -\frac{4\pi^2}{n} \left(I_n - \frac{1}{2} e_n e_n^T \right), \quad C = \frac{2\pi fi}{\zeta} e_n e_n^T, \quad K = n \begin{bmatrix} 2 & -1 & & \\ -1 & \ddots & \ddots & \\ & \ddots & 2 & -1 \\ & & -1 & 1 \end{bmatrix}.$$

We use `nlevp('acoustic_wave_1d', 1000, 1)` to generate these matrices with size $n = 1000$, impedance $\zeta = 1$ and wave speed $c = 1$.

- (3) *Concrete*. This quadratic eigenvalue problem is of the form $T(\lambda)v = (\lambda^2 M + \lambda C + (1 + i\mu)K)v = 0$, arising in a model of a concrete structure supporting a machine assembly [43]. The matrix M is real diagonal and of low rank. The viscous damping matrix C is pure imaginary and diagonal. The matrix K is complex symmetric, and the factor $(1 + i\mu)$ adds uniform hysteretic damping. These matrices are generated by `nlevp('concrete', 0.04)` with size $n = 2472$ and $\mu = 0.04$.
- (4) *String*. This rational eigenvalue problem arises in the finite element discretization of a boundary eigenvalue problem describing the eigenvibrations of a string with a load of unit mass attached by an elastic spring of unit stiffness [9]. It has the form $T(\lambda)v = (T_1 + \frac{\lambda}{\lambda-1}e_n e_n^T - \lambda T_3)v = 0$, where, n is the number of equally-spaced elements and

$$T_1 = n \begin{bmatrix} 2 & -1 & & \\ -1 & \ddots & \ddots & \\ & \ddots & 2 & -1 \\ & & -1 & 2 \end{bmatrix}, \quad T_3 = \frac{1}{6n} \begin{bmatrix} 4 & 1 & & \\ 1 & \ddots & \ddots & \\ & \ddots & 4 & 1 \\ & & 1 & 2 \end{bmatrix}.$$

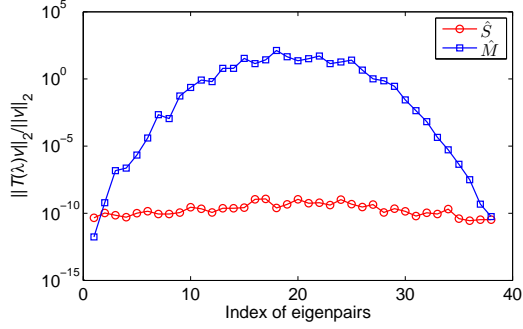
We use `nlevp('loaded_string', 5000, 1, 1)` to generate the matrices and compute 32 eigenvalues in the interval $[3, 10000]$. The size of this problem is $n = 5000$.

The controlling parameters of the CIRR algorithms used in the four problems are listed in Table 1. The N -point trapezoidal rule defined in the same way as (36) is used to compute the moments \hat{M} on the elliptical contour up to the order $K' = N$. The same set of quadrature points is used as the sampling points in \hat{S} as well. The orthogonal basis of the eigenspace is computed by using SVD. We do not truncate the SVD so that the dimensions of the resultant eigenspaces corresponding to \hat{S} and \hat{M} are maximal and have the same dimension. This should reflect the full power of the two eigenspaces respectively. To ensure the rank condition (29) and high accuracy in solving the reduced NEP, proper values of K and N_S are used, see the last two columns of Table 1.

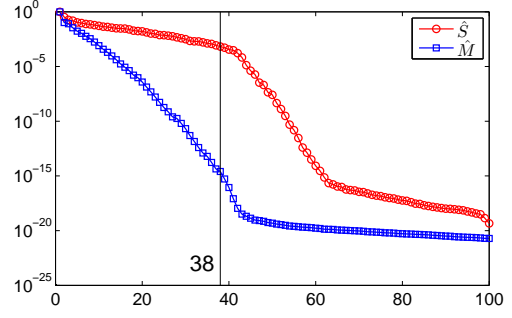
Table 1: Values of the controlling parameters of CIRR algorithms in four benchmark examples

	γ	(a, b)	L	N	K'	N_S	K
<i>Wiresaw</i>	60i	(6, 60)	1	100	100	1000	2
<i>Acoustic-1D</i>	$9.9 + 0.8i$	(10.1, 1.01)	2	100	100	1000	2
<i>Concrete</i>	$-1 + 52.5i$	(5.25, 52.5)	2	100	100	1000	2
<i>String</i>	5001.5	(4998.5, 249.925)	1	100	100	1000	8

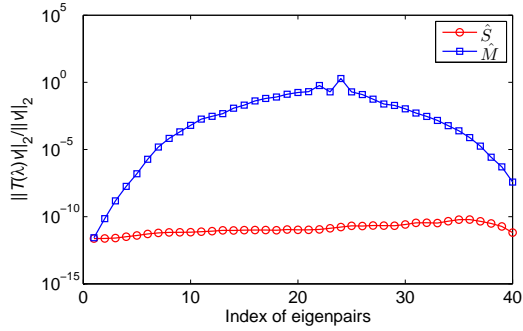
The numerical results are summarized and illustrated in Figure 3. For each example, the relative errors of the computed eigenpairs and the singular values of the matrices \hat{S} and \hat{M} are shown in one row. In illustrating the errors of eigenpairs, the eigenvalues are first sorted in ascending order according to their absolute values, then the error of each eigenpair is shown against its index in the sorted list; see the first



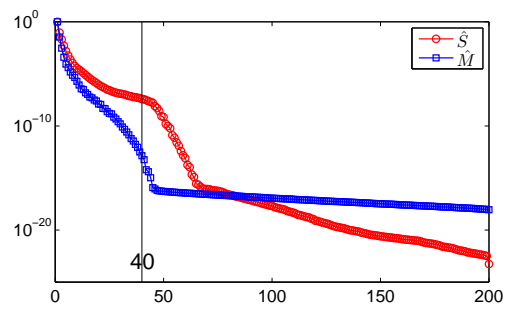
(a) Residuals of eigenpairs, *Wiresaw* example



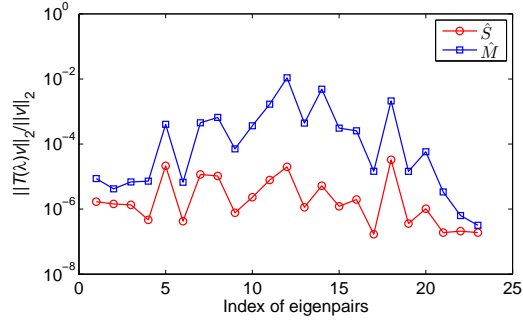
(b) Singular values of \hat{S} and \hat{M} , *Wiresaw* example



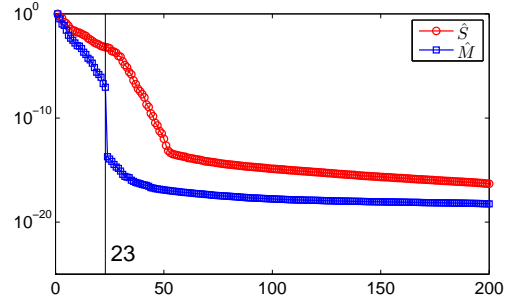
(c) Residuals of eigenpairs, *Acoustic-1D* example



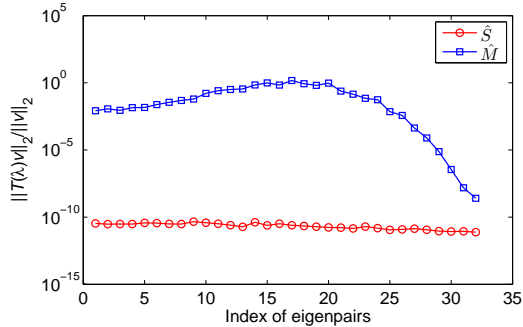
(d) Singular values of \hat{S} and \hat{M} , *Acoustic-1D* example



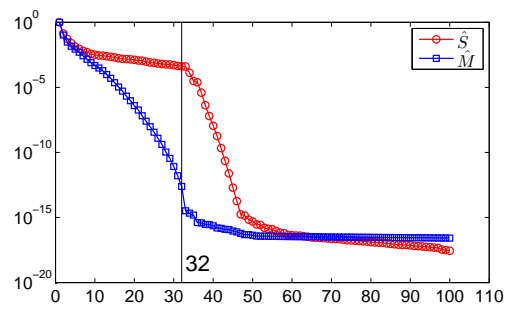
(e) Residuals of eigenpairs, *Concrete* example



(f) Singular values of \hat{S} and \hat{M} , *Concrete* example



(g) Residuals of eigenpairs, *String* example



(h) Singular values of \hat{S} and \hat{M} , *String* example

Figure 3: Comparison of the sampling scheme and the moment scheme for constructing eigenspaces for four benchmark examples.

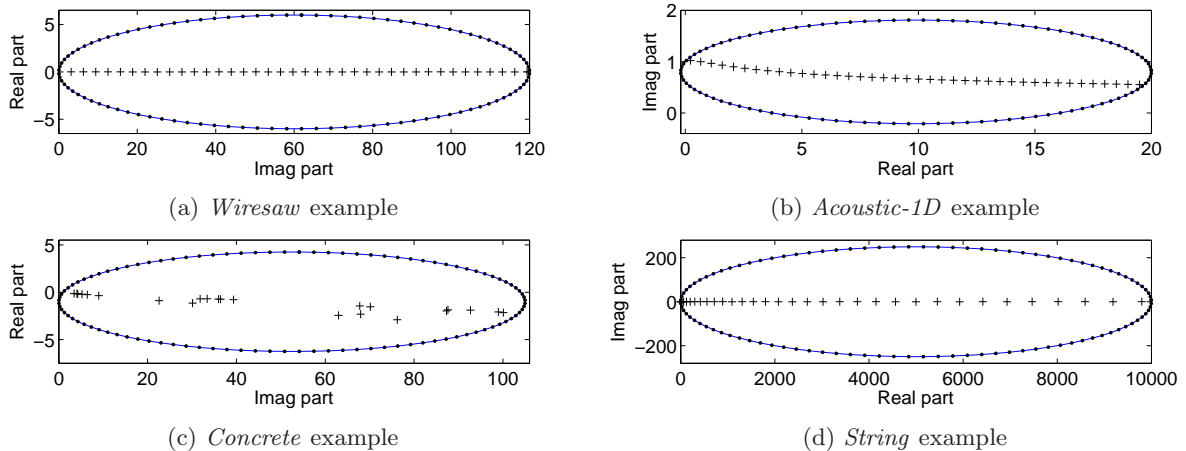


Figure 4: Computed eigenvalues (+) by using \hat{S} , contours (-) and sampling points (\bullet) of four benchmark examples. Note that in Figures 4a and 4c x -axis corresponds to the imaginary part while y -axis corresponds to the real part, which are different from Figures 4b and 4d.

column of Figure 3, i.e., plots (3a), (3c), (3e) and (3g). Clearly, the errors of eigenpairs computed by the CIRR(S) are typically several orders lower than the errors of their counterparts obtained by the CIRR(M). As explained in Section 3.1, this remarkable difference is caused by the distinct quality of eigenspaces obtained from \hat{S} and \hat{M} . To be specific, consider the behavior of singular values of \hat{S} and \hat{M} , as shown in plots (3b), (3d), (3f) and (3h) of Figure 3, where the singular values are scaled so that the first one is always 1. We use the vertical line in each plot to indicate the number of the eigenvalues \bar{n}_C . We see that, typically, the singular values of \hat{M} drop much faster than those of \hat{S} . In plots (3b), (3d) and (3h), the singular values of \hat{M} drop to around 10^{-15} at the \bar{n}_C -th singular value, indicating that the rank condition (10) cannot be satisfied with good accuracy. Whereas, the situation for \hat{S} is much better, and an obvious decay is observed only after the \bar{n}_C -th singular value. An exception can be seen from plot (3f), where the singular values of \hat{M} do not decay as fast as in the other examples (but still faster than \hat{S}). This may explain why the discrepancy between the errors of \hat{M} and \hat{S} in this example is not so remarkable as in the other examples.

In summary, the numerical results of these four benchmark examples confirm the basic claim in Section 3.1: the involvement of high order moments in \hat{M} can deteriorate the quality of the eigenspace, making it ill-conditioned and finally failed to ensure the rank condition (10) for proper extraction of eigenvalues. On the contrary, the matrix \hat{S} can always satisfy the condition (25) securely, leading to high quality eigenspaces. Our computation also indicates that, to achieve good eigenspace using \hat{S} , the sampling points on contour \mathcal{C} should be close to the eigenvalues so that they can be effectively “probed”. That’s why the contours in these examples are chosen to be oblate ellipses, see the column of (a, b) in Table 1. Figure 4 exhibits the locations of the contour sampling points and the computed eigenvalues by using \hat{S} .

Finally, we remark that in all these four examples the values of L and N in Table 1 are chosen to ensure that the correct number of the eigenvalues \bar{n}_C can be determined by using the moment scheme, i.e., \hat{M} . As we have seen, in this case \hat{S} always performs much better than \hat{M} . But those values are by no means optimal for \hat{S} . For example, we have used $L = 2$ in the *Acoustic-1D* example before. If we use $L = 1$, the 40 correct eigenpairs can still be accurately extracted by using \hat{S} with almost the same accuracy as shown in Figure 3c. However, by using \hat{M} , only 32 “eigenpairs” are obtained and most of them are incorrect.

7.2. BEM example

To exhibit the potential of the CIRR(S) method in BEM applications, a more engineering oriented example, the acoustic modal analysis of a car cabin cavity, is performed. The BEM linear systems $T(z_p)^{-1}U$, $p = 1, \dots, N$ are solved by using the GMRES solver with ILU preconditioner. Both the accuracy of the fast BEM and the convergence tolerance of the GMRES solver are set to be 10^{-6} . The matrix $T(\lambda)$ is interpolated

by using Chebyshev polynomials of degree $d = 40$. In solving the reduced NEPs, parameters $N_S = 500$ and $K = 2$ are used.

The boundary of the car cabin cavity is partitioned into 9850 triangular quadratic elements, leading to a BEM model with 59100 DOF; see Figure 5. The entire boundary is assumed to be rigid, i.e., $q = 0$. We solve for the eigenvalues in the interval $[40, 500]$ Hz. The contour is chosen to be the ellipse defined by $\gamma = 270$, $a = 230$ and $b = 0.1a$. Other controlling parameters of the CIRR are set as: $L = 2$, $N = 200$. It turns out that there are 64 eigenvalues in this interval.

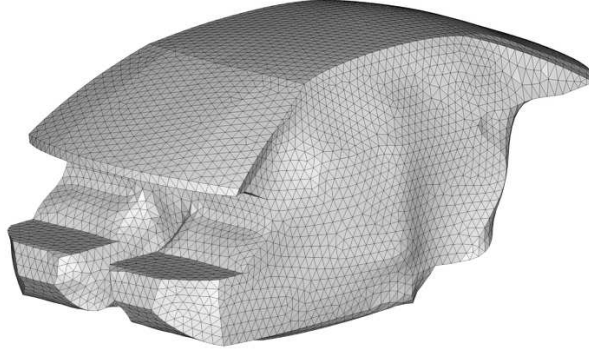


Figure 5: BEM mesh of the car cabin model

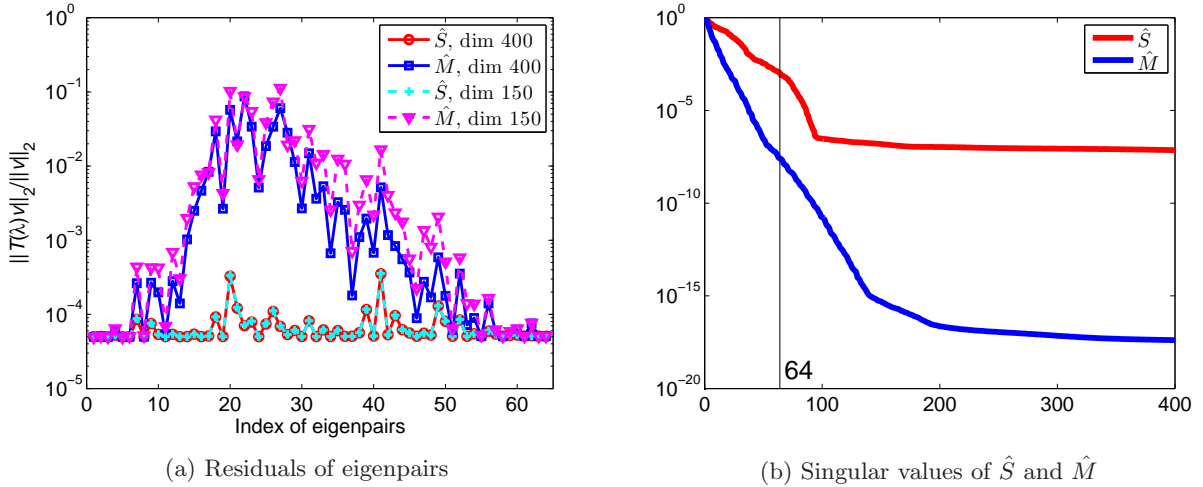


Figure 6: Comparison of the sampling scheme and moment scheme for constructing eigenspace for the car cabin model.

To test the performance of the two schemes for constructing eigenspace in the BEM. We consider two cases. In one case, the SVDs of \hat{S} and \hat{M} are both not truncated, so the dimensions of the eigenspaces are all 400. In another case, the SVDs of \hat{S} and \hat{M} are truncated so that the dimensions of the eigenspaces are all 150. The relative errors $\|T(\lambda)v\|_2/\|v\|_2$ of the computed 64 eigenpairs are shown in Figure 6a. Similar to previous results, the sampling scheme performs much better than the moment scheme. When decreasing the dimension of the eigenspace from 400 to 150, no obvious increase of error is observed for the sampling scheme, indicating that the eigenspace information is effectively concentrated to the singular vectors of \hat{S} associated with large singular values. But for the moment scheme, increasing the dimension

of the eigenspace slightly improved the results; however, even when using the largest eigenspace (dimension 400), most eigenpairs at the middle part of the spectral are still of very low accuracy. Figure 6b shows the behaviors of the singular values of \hat{S} and \hat{M} .

7.3. FEM examples

The CIRR(S) algorithm is applied to solve typical NEPs in engineering finite element analysis. We consider two models. The first is a viscoelastic sandwich plate model, mainly used to confirm the superiority of the newly proposed sampling scheme in eigenspace generation. The second is a large-scale model consisting of around one million DOF. The engineering background of this model is the payload attach fitting structure used between the satellite and the launch vehicle for vibration isolation purpose.

The finite element analysis part in these two examples is conducted using ANSYS®. The linear systems in computing $T(z_p)^{-1}U$ are solved by using the sparse LU decomposition solver in ANSYS®, and the accuracy of the solutions is always above 6 significant digits. In solving the reduced NEPs we use $N_S = 500$, $K = 2$.

7.3.1. Viscoelastic sandwich plate

The viscoelastic sandwich plate model shown in Figure 7 is selected from [44] (Section 4.1). It consists of three layers. The base layer and constraining layer are Steel and Aluminum, respectively. In between these two layers is a layer of viscoelastic damping material which is modeled by using the Biot model. The plate is fixed at one side in the longest direction and free at the other sides. The sizes and material parameters are given in Table 2. The structure is discretized by using SOLID186 element (20-node hexahedral element exhibiting quadratic displacement behavior), leading to an analysis model with 18180 DOF. The system matrix of the NEP is given by

$$T(z) = z^2 M + G(z)K_v + K, \quad \text{and} \quad G(z) = G_\infty \sum_{k=1}^3 \frac{a_k z}{z + b_k}, \quad (46)$$

where, M and K are the conventional mass matrix and stiffness matrix, K_v is the unit viscoelastic stiffness matrix, the three matrices are all of dimension 18180, $G_\infty = 3.441 \times 10^5$ Pa, $a_1 = 2.06$, $a_2 = 67.1985$, $a_3 = 506.9457$, $b_1 = 193.39$ rad/s, $b_2 = 16345$ rad/s and $b_3 = 485918.4$ rad/s.

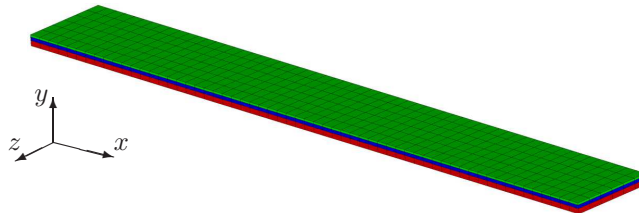


Figure 7: FEM mesh of the viscoelastic sandwich plate model. The model consists of three layers from top to bottom: the constraining layer, the damping layer and the base layer.

Table 2: The geometry and material parameters of the three-layer sandwich plate [44].

Parameters	Base layer	Damping layer	Constraining layer
x -length (mm)	400	400	400
y -length (mm)	50	50	5
z -length (mm)	3	2	1.2
Elastic modulus (Pa)	2.085×10^{11}	1.0254×10^6	6.76×10^{10}
Density (kg/m^3)	7840	789.5	2803
Poisson's ratio	0.3	0.49	0.3

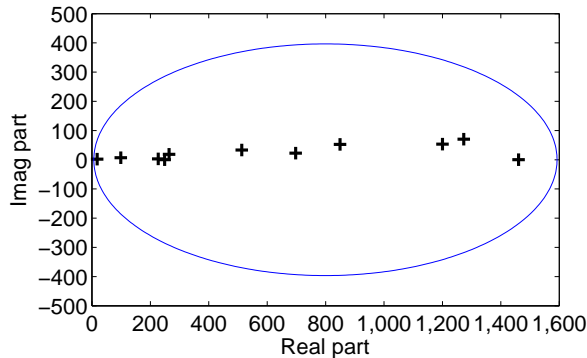
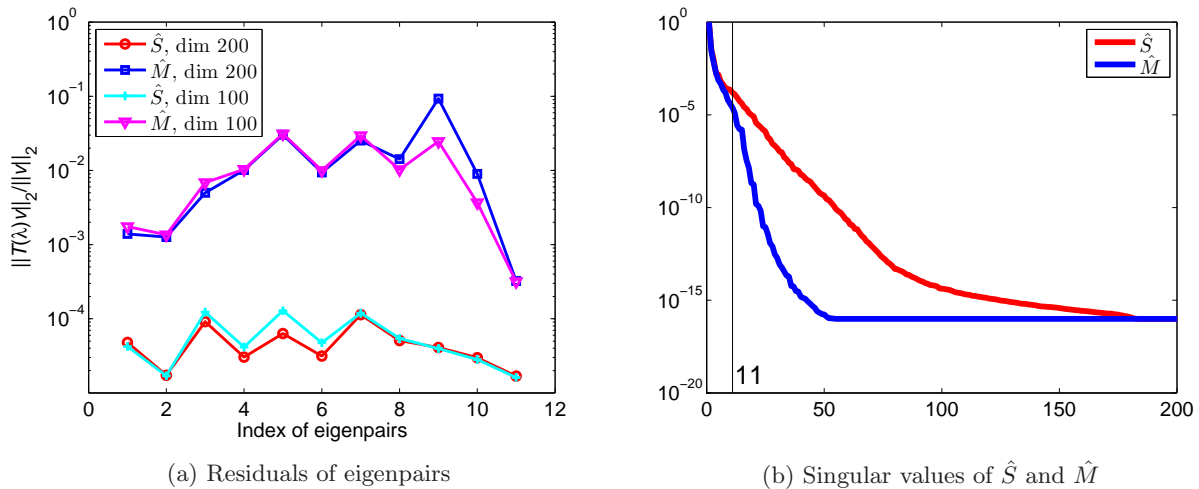


Figure 8: Computed eigenvalues (+) and the contour (-) of the viscoelastic sandwich plate model

We solve for the natural frequencies in the interval $[6.4, 1592.4]$ Hz. The contour is chosen to be the ellipse defined by $\gamma = 799.4$, $a = 793$, $b = 0.5a$. Other controlling parameters of CIRR algorithms are set as: $L = 2$, $N = 200$, $K = N$. We obtain 11 eigenpairs by using the CIRR(S); see Figure 8 for the distribution of the computed eigenvalues. The relative error $\|T(\lambda)v\|_2/\|v\|_2$ of the computed eigenpairs is illustrated in Figure 9a, and the behavior of the singular values of the matrices \hat{S} and \hat{M} is illustrated in Figure 9b. Note that both \hat{S} and \hat{M} should have 400 singular values, but only the first 200 singular values are shown in Figure 9b because the remainders are almost constant around 10^{-16} .



(a) Residuals of eigenpairs

(b) Singular values of \hat{S} and \hat{M}

Figure 9: Comparison of the sampling scheme and moment scheme for the viscoelastic sandwich plate model. In the left plot, “dim” indicates the dimension of the eigenspace.

To test the performance of \hat{S} and \hat{M} in generating eigenspace, the SVDs of them are truncated so that the dimensions of the resultant eigenspaces are 200 and 100, respectively. From Figure 9a, one can see that the errors of the sampling scheme are typically below 10^{-4} , one order lower than those of the moment scheme. In addition, for both the two schemes, the change in the dimension of the eigenspaces does not lead to an obvious change in the errors of the eigenpairs. In view of the singular value behavior in Figure 9b, this indicates that it is sufficient to truncate the SVD by $\delta = 10^{-14}$. In a nutshell, one can see that the sampling scheme can provide eigenspaces with much better quality than the moment scheme, provided that the SVD of \hat{S} is truncated by $\delta < 10^{-14}$. Our further numerical tests also show that the errors corresponding to the sampling scheme tend to increase with the increase of $\delta > 10^{-14}$. Similar behavior can also be observed in

the moment scheme.

7.3.2. Payload attach fitting

As a large-scale example, we consider the payload attach fitting model illustrated in Figure 10. This kind of structure usually serves as an isolator between the satellite and the launch vehicle to reduce the satellite vibration caused by the launch-induced dynamic loads. The structural material is Aluminum with elastic modulus 70 GPa, density 2770 kg/m³ and Poisson's ratio 0.3. The viscoelastic damping material in the damping cylinder is ZN1 polymer which is modeled by using the Biot model. The density and Poisson's ratio of the damping material are 970 kg/m³ and 0.49, respectively. The structure is fixed at the lower surface of the damping flange and all other surfaces are free of traction. The model is discretized by using SOLID186 element, and the total number of DOF is 1005648. The expression of this NEP is the same as that in (46), but with $G(z) = G_\infty \left(1 + \sum_{k=1}^4 \frac{a_k z}{z + b_k}\right)$, where $G_\infty = 362750$ Pa, $a_1 = 0.762063$, $a_2 = 1.814626$, $a_3 = 84.93828$, $a_4 = 4.869723$, $b_1 = 53.72964$, $b_2 = 504.5871$, $b_3 = 29695.64$ and $b_4 = 2478.43$.

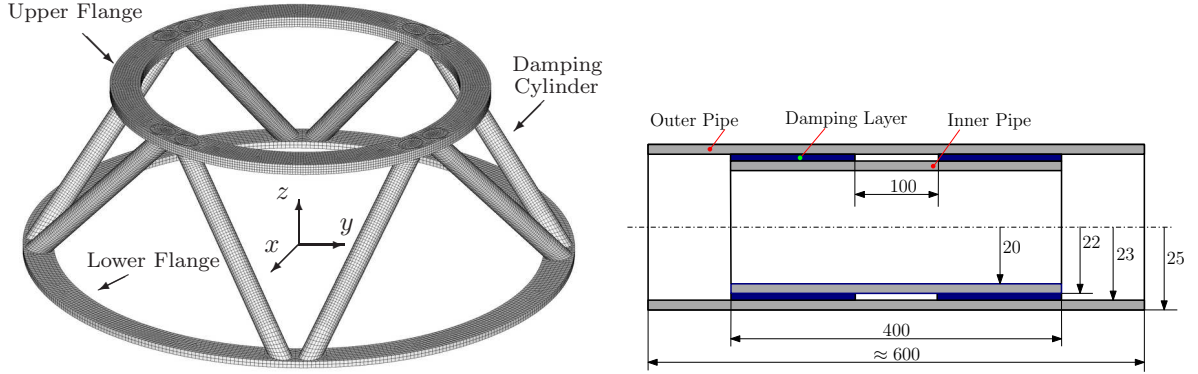


Figure 10: Payload attach fitting model (Unit: mm). The model consists of an upper flange, a lower flange and eight damping cylinders. The dimensions of the upper flange are: radius of inner circle 365, radius of outer circle 435, thickness 24. The dimensions of the lower flange are: radius of inner circle 560, radius of outer circle 630, thickness 16. The structure and dimensions of the damping cylinders are shown in the left diagram.

Natural frequencies below 640Hz are sought. A rough modal analysis of the undamped structure shows that the lowest natural frequency is around 200 Hz. So we set the frequency interval of the CIRR(S) to be [160, 640]Hz. The ellipse contour with $\gamma = 400$, $a = 240$ and $b = 0.5a$ is used accordingly. Besides, we let $L = 2$ and $N = 100$. Thus there are totally 200 FEM linear systems to be solved.

The computation was carried out on a Server with eight 8-core Intel Xeon (2.67GHz) processors. The whole solution process takes about 7 hours. There are 14 eigenpairs in the interval; see Table 3 for the eigenfrequencies and the corresponding errors. Due to the symmetry of the structure, there are 3 couples of 2-fold eigenfrequencies. The largest error is around 10^{-5} , indicating a good accuracy of the CIRR(S) for solving real-world problems. We believe that for this problem the accuracy of the computed eigenpairs is mainly limited by that of the linear system solver (sparse LU decomposition) in ANSYS®, because a largest relative error of around 10^{-6} was observed by us in solving the 200 linear systems. Nevertheless, an accuracy of 5 significant digits should be sufficient for most engineering applications. Figure 11 exhibits the amplitude of the first 6 modes of the model. Clearly, modes 2 and 3 correspond to a 2-fold frequency and so they are symmetric with each other. Modes 1, 4 and 5 correspond to simple eigenfrequencies, each of them is symmetric with respect to z -axis that passes through the centers of the lower and upper flanges. Analogously, mode 6 should be symmetric with mode 7 which is not illustrated.

Table 3: Computed eigenvalues with errors of the payload attach fitting model

k	λ_k	$\ T(\lambda)v\ _2/\ v\ _2$	k	λ_k	$\ T(\lambda)v\ _2/\ v\ _2$
1	$206.88 + 0.99i$	3.80×10^{-6}	8	$405.56 + 8.45i$	1.93×10^{-6}
2	$228.06 + 1.79i$	5.99×10^{-6}	9	$431.31 + 12.26i$	3.60×10^{-6}
3	$228.06 + 1.79i$	1.14×10^{-5}	10	$551.31 + 6.26i$	4.80×10^{-7}
4	$251.95 + 0.16i$	1.54×10^{-5}	11	$551.31 + 6.26i$	3.21×10^{-6}
5	$289.73 + 2.91i$	1.70×10^{-7}	12	$573.46 + 2.98i$	3.50×10^{-7}
6	$345.70 + 12.25i$	2.93×10^{-6}	13	$607.30 + 15.48i$	2.75×10^{-6}
7	$345.70 + 12.25i$	3.46×10^{-6}	14	$630.17 + 17.92i$	1.51×10^{-6}

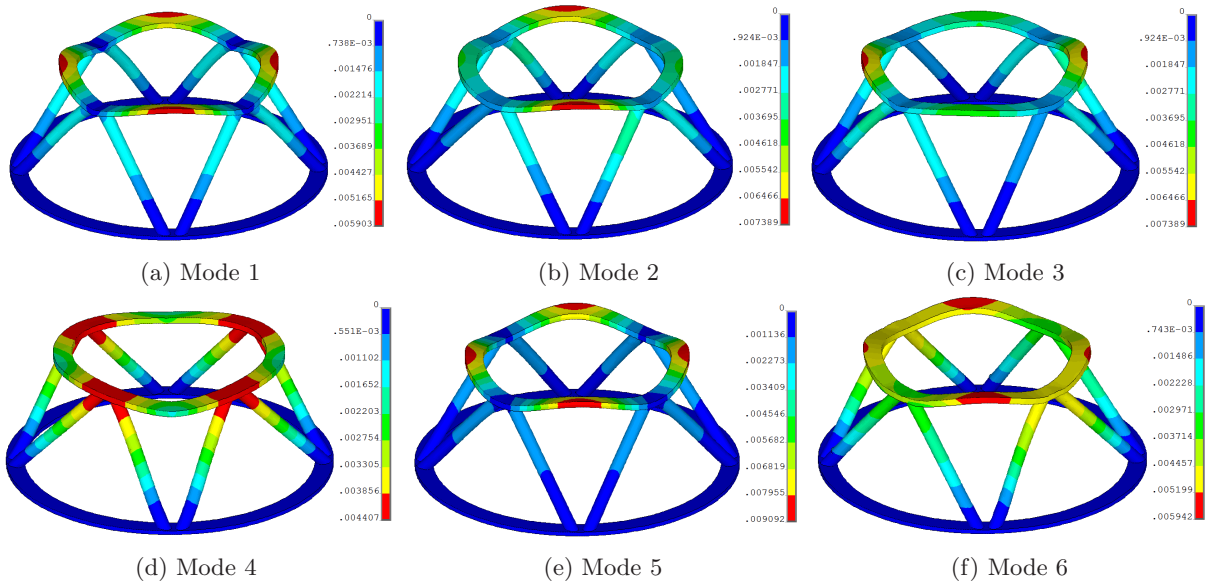


Figure 11: Amplitude of the first 6 modes of the payload attach fitting model.

8. Conclusions

This paper is devoted to the efficient numerical methods for solving large-scale NEPs of the type $T(\lambda)v = 0$ in computational science and engineering. The outcome is a robust and reliable method, denoted by CIRR(S), which is suitable for general NEPs no matter the matrix T is sparse or dense, structured or unstructured. The method is based on the Rayleigh-Ritz procedure. We have proposed a new sampling scheme for generating reliable eigenspaces using the contour integral method, and a modified block SS algorithm for robust and accurate solution of the reduced NEP. The main computational work of the CIRR(S) lies in the solution of independent linear systems with T for a series of λ values. But this operation is very suitable for parallelization and in many areas fast linear solvers are available.

As applications, the CIRR(S) algorithm has been used to solve representative NEPs in engineering finite element and boundary element analysis. Note that the application to the latter is not straightforward. The Chebyshev interpolation technique has been employed to obtain approximate expressions for the matrix $T(\lambda)$ and its reduced counterpart. The good performance of the newly proposed sampling scheme in generating eigenspaces and finally the robustness, reliability and accuracy of the CIRR(S) have been attested by several NEPs in a variety of applications. In addition, the potential of the CIRR(S) in large-scale simulation has been demonstrated by solving a FEM NEP with 1 million DOF and a BEM NEP with 60 thousand DOF. A major computational advantage offered by the CIRR(S) algorithm is that it is very easily parallelizable. Besides, it can be easily implemented into other programs and softwares.

Acknowledgements

JX gratefully acknowledges the financial supports from the National Science Foundations of China under Grants 11102154 and 11472217, Fundamental Research Funds for the Central Universities and the Alexander von Humboldt Foundation (AvH) to support his fellowship research at the Chair of Structural Mechanics, University of Siegen, Germany.

References

References

- [1] F. Tisseur, K. Meerbergen, The quadratic eigenvalue problem, *SIAM review* 43 (2) (2001) 235–286.
- [2] V. Mehrmann, H. Voss, Nonlinear eigenvalue problems: A challenge for modern eigenvalue methods, *GAMM-Mitteilungen* 27 (2) (2004) 121–152.
- [3] V. Mehrmann, C. Schröder, Nonlinear eigenvalue and frequency response problems in industrial practice, *Journal of Mathematics in Industry* 1 (1) (2011) 1–18.
- [4] T. van Opstal, E. van Brummelen, G. van Zwieten, A finite-element/boundary-element method for three-dimensional, large-displacement fluid–structure–interaction, *Computer Methods in Applied Mechanics and Engineering* 284 (2015) 637–663.
- [5] A. Kimeswenger, O. Steinbach, G. Unger, Coupled finite and boundary element methods for fluid-solid interaction eigenvalue problems, *SIAM Journal on Numerical Analysis* 52 (5) (2014) 2400–2414.
- [6] E. Daya, M. Potier-Ferry, A numerical method for nonlinear eigenvalue problems application to vibrations of viscoelastic structures, *Computers & Structures* 79 (5) (2001) 533–541.
- [7] F. Cortés, M. J. Elejabarrieta, Computational methods for complex eigenproblems in finite element analysis of structural systems with viscoelastic damping treatments, *Computer Methods in Applied Mechanics and Engineering* 195 (44) (2006) 6448–6462.
- [8] S. Adhikari, B. Pascual, Eigenvalues of linear viscoelastic systems, *Journal of Sound and Vibration* 325 (4) (2009) 1000–1011.
- [9] S. I. Solov'ev, Preconditioned iterative methods for a class of nonlinear eigenvalue problems, *Linear Algebra and its Applications* 415 (1) (2006) 210–229.
- [10] C. Conca, J. Planchard, M. Vanninathan, Existence and location of eigenvalues for fluid-solid structures, *Computer Methods in Applied Mechanics and Engineering* 77 (3) (1989) 253–291.
- [11] M. Botchev, G. Sleijpen, A. Sopaheluwakan, An SVD-approach to Jacobi–Davidson solution of nonlinear Helmholtz eigenvalue problems, *Linear Algebra and its Applications* 431 (3) (2009) 427–440.
- [12] S. M. Kirkup, S. Amini, Solution of the Helmholtz eigenvalue problem via the boundary element method, *International Journal for Numerical Methods in Engineering* 36 (2) (1993) 321–330.
- [13] A. Ali, C. Rajakumar, S. Yunus, Advances in acoustic eigenvalue analysis using boundary element method, *Computers & Structures* 56 (5) (1995) 837–847.
- [14] O. Steinbach, G. Unger, Convergence analysis of a Galerkin boundary element method for the Dirichlet Laplacian eigenvalue problem, *SIAM Journal on Numerical Analysis* 50 (2) (2012) 710–728.
- [15] C. Effenberger, D. Kressner, Chebyshev interpolation for nonlinear eigenvalue problems, *BIT Numerical Mathematics* 52 (4) (2012) 933–951.
- [16] C. Effenberger, Robust successive computation of eigenpairs for nonlinear eigenvalue problems, *SIAM Journal on Matrix Analysis and Applications* 34 (3) (2013) 1231–1256.
- [17] C. Effenberger, D. Kressner, O. Steinbach, G. Unger, Interpolation-based solution of a nonlinear eigenvalue problem in fluid–structure interaction, *PAMM* 12 (1) (2012) 633–634.
- [18] H. Voss, An Arnoldi method for nonlinear eigenvalue problems, *BIT numerical mathematics* 44 (2) (2004) 387–401.
- [19] H. Voss, A Jacobi–Davidson method for nonlinear and nonsymmetric eigenproblems, *Computers & Structures* 85 (17) (2007) 1284–1292.
- [20] D. Kressner, A block Newton method for nonlinear eigenvalue problems, *Numerische Mathematik* 114 (2) (2009) 355–372.
- [21] W.-J. Beyn, An integral method for solving nonlinear eigenvalue problems, *Linear Algebra and Its Applications* 436 (10) (2012) 3839–3863.
- [22] R. Van Beeumen, K. Meerbergen, W. Michiels, A rational Krylov method based on Hermite interpolation for nonlinear eigenvalue problems, *SIAM Journal on Scientific Computing* 35 (1) (2013) A327–A350.
- [23] A. Neumaier, Residual inverse iteration for the nonlinear eigenvalue problem, *SIAM Journal on Numerical Analysis* 22 (5) (1985) 914–923.
- [24] T. Betcke, H. Voss, A Jacobi–Davidson-type projection method for nonlinear eigenvalue problems, *Future Generation Computer Systems* 20 (3) (2004) 363–372.
- [25] N. Kamiya, E. Andoh, K. Nogae, A new complex-valued formulation and eigenvalue analysis of the Helmholtz equation by boundary element method, *Advances in Engineering Software* 26 (3) (1996) 219–227.
- [26] D. Kressner, J. E. Roman, Memory-efficient arnoldi algorithms for linearizations of matrix polynomials in Chebyshev basis, *Numerical Linear Algebra with Applications* 21 (4) (2014) 569–588.

- [27] D. S. Mackey, N. Mackey, C. Mehl, V. Mehrmann, Structured polynomial eigenvalue problems: Good vibrations from good linearizations, *SIAM Journal on Matrix Analysis and Applications* 28 (4) (2006) 1029–1051.
- [28] Y. Cao, L. Wen, J. Xiao, Y. Liu, A fast directional BEM for large-scale acoustic problems based on the Burton–Miller formulation, *Engineering Analysis with Boundary Elements* 50 (2015) 47–58.
- [29] T. Sakurai, H. Sugiura, A projection method for generalized eigenvalue problems using numerical integration, *Journal of Computational and Applied Mathematics* 159 (1) (2003) 119–128.
- [30] E. Polizzi, Density-matrix-based algorithm for solving eigenvalue problems, *Physical Review B* 79 (11) (2009) 115112.
- [31] T. Sakurai, J. Asakura, H. Tadano, T. Ikegami, Error analysis for a matrix pencil of Hankel matrices with perturbed complex moments, *JSIAM Letters* 1 (0) (2009) 76–79.
- [32] H. Gao, T. Matsumoto, T. Takahashi, H. Isakari, Eigenvalue analysis for acoustic problem in 3D by boundary element method with the block Sakurai–Sugiura method, *Engineering Analysis with Boundary Elements* 37 (6) (2013) 914–923.
- [33] A. Leblanc, A. Lavie, Solving acoustic nonlinear eigenvalue problems with a contour integral method, *Engineering Analysis with Boundary Elements* 37 (1) (2013) 162–166.
- [34] C.-J. Zheng, H.-B. Chen, H.-F. Gao, L. Du, Is the Burton–Miller formulation really free of fictitious eigenfrequencies?, *Engineering Analysis with Boundary Elements* 59 (2015) 43–51.
- [35] T. Sakurai, H. Tadano, et al., CIRR: a Rayleigh-Ritz type method with contour integral for generalized eigenvalue problems, *Hokkaido Mathematical Journal* 36 (4) (2007) 745–757.
- [36] S. Yokota, T. Sakurai, A projection method for nonlinear eigenvalue problems using contour integrals, *JSIAM Letters* 5 (0) (2013) 41–44.
- [37] M. Bilasse, I. Charpentier, Y. Koutsawa, et al., A generic approach for the solution of nonlinear residual equations. Part II: Homotopy and complex nonlinear eigenvalue method, *Computer Methods in Applied Mechanics and Engineering* 198 (49) (2009) 3999–4004.
- [38] R. Mennicken, M. Möller, Non-self-adjoint boundary eigenvalue problems, *North-Holland Mathematics Studies*, Vol. 192, North-Holland Publishing Co., Amsterdam, 2003.
- [39] J. Asakura, T. Sakurai, H. Tadano, T. Ikegami, K. Kimura, A numerical method for nonlinear eigenvalue problems using contour integrals, *JSIAM Letters* 1 (0) (2009) 52–55.
- [40] J.-P. Berrut, L. N. Trefethen, Barycentric Lagrange interpolation, *SIAM Review* 46 (3) (2004) 501–517.
- [41] A. P. Austin, P. Kravanja, L. N. Trefethen, Numerical algorithms based on analytic function values at roots of unity, *SIAM Journal on Numerical Analysis* 52 (4) (2014) 1795–1821.
- [42] T. Betcke, N. J. Higham, V. Mehrmann, C. Schröder, F. Tisseur, NLEVP: A collection of nonlinear eigenvalue problems, *ACM Transactions on Mathematical Software (TOMS)* 39 (2) (2013) 7.
- [43] A. Feriani, F. Perotti, V. Simoncini, Iterative system solvers for the frequency analysis of linear mechanical systems, *Computer Methods in Applied Mechanics and Engineering* 190 (13) (2000) 1719–1739.
- [44] L. Li, Y. Hu, X. Wang, Harmonic response calculation of viscoelastic structures using classical normal modes: An iterative method, *Computers & Structures* 133 (2014) 39–50.